WATER SCIENCE SERIES

Integrated Hydrological Model for Windermere Creek Watershed: Groundwater Dynamics and Connectivity with Surface Water

Alexandre H. Nott, Diana M. Allen and Natasha Neumann

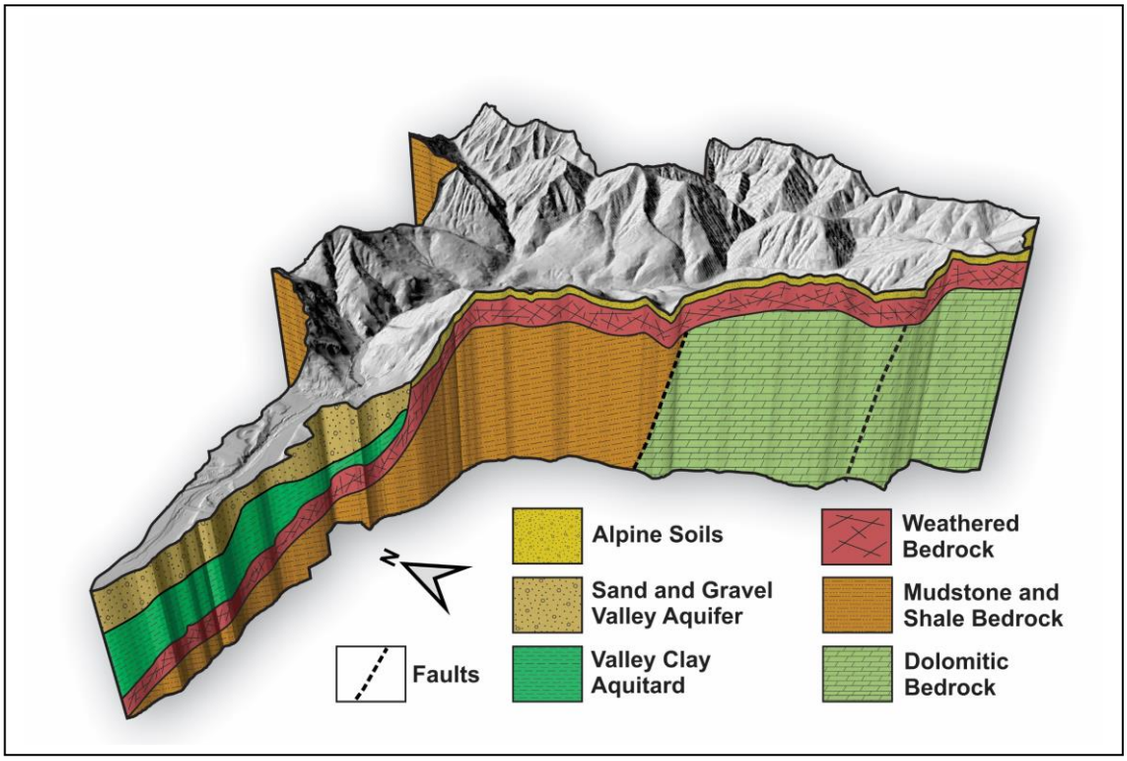

November 2023

BRITISH COLUMBIA

SFU SIMON FRASER UNIVERSITY

No. 2023-02

The **Water Science Series** are scientific technical reports relating to the understanding and management of B.C.'s water resources. The series communicates scientific knowledge gained through water science programs across B.C. government, as well as scientific partners working in collaboration with provincial staff. For additional information visit: http://www2.gov.bc.ca/gov/content/environment/air-land-water/water/water-science-data/water-science-series.

ISBN: 978-1-0399-0075-2

Citation:
Nott, A.H., D.M. Allen and N. Neumann. 2023. Integrated Hydrological Model for Windermere Creek Watershed: Groundwater Dynamics and Connectivity with Surface Water. Water Science Series, WSS2023-02. Province of B.C., Victoria.

Author's Affiliation:
A. Nott, MSc. Student
Department of Earth Sciences
Simon Fraser University

D.M. Allen, P.Geo., Professor
Department of Earth Sciences
Simon Fraser University

Natasha Neumann, P.Ag., Research Hydrologist
British Columbia Ministry of Forests
Adjunct Professor, Department of Earth, Environmental and Geographic Sciences
University of British Columbia Okanagan

Cover Image:
Hydrogeological conceptual model of the Windermere Creek Watershed

Acknowledgements

Funding for this research was provided by the British Columbia Ministry of Forests. The authors acknowledge Living Lakes Canada for providing the digital geological model files (Leapfrog Geo files) prepared by GW Solutions as part of the study "Windermere Preliminary Hydrogeological Characterization". We would also like to thank Chris Donnelly for the comments on this report.

EXECUTIVE SUMMARY

This study focuses on the seasonal and interannual groundwater dynamics and connectivity with surface water in Windermere Creek Watershed (WCW). The study was motivated by concerns raised by local residents about recharge sources and groundwater sustainability in the fan area, as well as a need for better understanding of the connectivity between the creek and unconfined aquifer for fish habitat restoration.

A three-dimensional integrated hydrological model of WCW was developed using the software MIKE SHE, with the aim of quantifying the water balance for the watershed, identifying recharge and discharge areas and where exchanges between surface water and groundwater occur, estimating the contribution of groundwater to stream baseflow, and exploring the seasonal/interannual variability in these processes.

An existing 3D hydrostratigraphic model of the alluvial fan, developed in Leapfrog by GW Solutions (2021) and commissioned by Living Lakes Canada, was used to represent the hydrogeological units in the fan area. Unfortunately, the lack of a direct interface between the two proprietary software packages, Leapfrog and MIKE SHE, meant that the Leapfrog files could not be directly imported into MIKE SHE. Therefore, a novel approach was developed for representing the subsurface in MIKE SHE via the use of geological lenses. This approach could be used in future modelling studies.

The model domain encompassed the Windermere catchment, extending from high elevation in the mountain block, through the fan at low elevations, to the outlet at Windermere Lake. An attempt was made to expand the model domain to better capture mountain front processes related to the triangular facets of the mountain faces as well as incorporating some domestic well users outside the catchment. However, the model was unstable and failed to properly run, as overland flow was not properly being routed. A conventional model calibration procedure could not be done due to a lack of data on the physical parameters (i.e., hydraulic conductivity and storage) representing the soils, aquifers, and streambed sediment. More importantly, there was a significant lack of data with which to calibrate the model. There are no modern timeseries data for climate, snow, streamflow or groundwater levels within the bounds of the catchment. Therefore, the calibration process involved adjusting model parameters to best simulate snow accumulation and melt, and streamflow based on sparse nearby or near-in-time data.

Despite the lack of conventional model calibration, the final model performed well at capturing the seasonality and large-scale spatial patterns of groundwater levels and flow patterns. Actual evapotranspiration (AET) represents about 31% of precipitation while overland (OL) flow represents about 20% of precipitation. Recharge in MIKE SHE represents the transfer of water from the unsaturated zone (UZ) to the saturated zone (SZ). About 91% of precipitation results in infiltration from rainfall and snowmelt. Because water may transfer back and forth several times in any model time step between the UZ and the SZ, the recharge estimate is over-estimated. Therefore, a more realistic estimate of recharge on the order of 60% of precipitation was calculated using the individually modelled components of the model (AET and Infiltration (I)).

Model results suggest Windermere Creek is consistently gaining water from groundwater in both space and time. Unfortunately, baseflow to Windermere Creek was consistently underestimated, although peak flows and flow recessions followed the expected patterns of timing. In the fan area, there is likely strong hydraulic connectivity between the fan aquifer and Windermere Creek; however, spatial and temporal exchanges could not be resolved with a model of this scale (50 m grid size). There are likely localized exchanges within the stream that could be resolved if a smaller scale model is developed for

the fan area in the future. The model also suggests groundwater seepage zones in the valley within the fan and in the wetland area at the fan apex.

Overall, the WCW is severely data starved, which resulted in uncertain modelling results. Nevertheless, the catchment scale model has provided a baseline for future detailed studies including, for example, a local scale model of the fan. A small-scale model would be more appropriate for exploring fish habitat suitability and localized interactions between aquifers and the stream. However, the model would require substantial physical and timeseries data including snowpack data measured at high and low elevation; groundwater level data from permanent monitoring wells, especially near the stream; and streamflow and vertical flux (exchange) along the stream using stream gauges installed at different locations along the stream in the fan area and instream piezometers.

CONTENTS

EXECUTIVE SUMMARY II
1. INTRODUCTION 1
2. CATCHMENT SCALE INTEGRATED HYDROLOGICAL MODEL 2
2.1 Overview of the Modelling Software 2
2.2 Topography 3
2.3 Climate and Weather 5
2.4 Land Use and Vegetation 7
2.5 Overland Flow 9
2.6 Streamflow 9
2.7 Geology and Groundwater 12
2.8 Model Structure and Parameterization 16
2.8.1 Saturated Zone 16
2.8.2 Unsaturated Zone 18
2.9 Simulation Specifications 20
2.10 Model Calibration 20
3. RESULTS 22
3.1 Precipitation and Snow Storage 22
3.2 Mean Groundwater Levels 24
3.3 Recharge and Discharge 27
3.4 Annual Water Balances 31
3.5 Mean Monthly Water Balance 33
3.6 GW-SW Interactions 35
3.7 Wet vs. Dry Water Year 40
4. DISCUSSION 44
4.1 Groundwater Recharge and Discharge 44
4.2 Groundwater Use and Climate Change 45
CONCLUSIONS AND RECOMMENDATIONS 48
REFERENCES 49

FIGURES

Figure 1: Windermere Creek Watershed (WCW). The locations of the hydrometric station, two climate stations and Living Lakes Canada observation wells are shown. 3
Figure 2: Summary of DEM mosaicking workflow in QGIS for joining a high- and low-resolution DEM..... 4
Figure 3: Complex topography of the WCW fan visible using the LiDAR-derived 1m DEM. 5
Figure 4: Climate normals (1991-2020) for the Toby Climate Station (FLNRORD 417) in Invermere. 6
Figure 5: Mean daily snow water equivalent (SWE) from a) the Three Isle Lake snow pillow station 53 km east of Windermere, and b) the Floe Lake snow weather station 67 km north of Windermere. 7
Figure 6: 2015 Land Cover of Canada classes within the study area. 8
Figure 7: Windermere Creek hydrograph (ECCC Station 08NA024) showing daily statistics for the period 1959-1979.. 10
Figure 8: Windermere Creek monthly flows (ECCC Station 08NA024) from 1959 to 1979. 10
Figure 9: WCW MIKE HYDRO River stream network. 11
Figure 10: Bedrock geology of the WCW. 12
Figure 11: Sediment thickness in the WCW valley. 13
Figure 12: Geological conceptual model of the WCW. 14
Figure 13: Meteorological and SWE data for 2018-2021. 15
Figure 14: Hydrostratigraphic model structure for the WCW. 16
Figure 15: Computational layers and hydraulic conductivity distribution along a transect of the valley centre. 18
Figure 16: Soil textural classes from the BC soil survey for the unsaturated zone in the WCW. 19
Figure 17: (**a**) Simulated (WCW) and observed (Floe Lake Station) SWE and (**b**) simulated and observed (Windermere Creek Gauge) streamflow. 21
Figure 18. Average daily precipitation rate in the WCW. 23
Figure 19. Average annual total snow storage in the WCW. 24
Figure 20: Average hydraulic head (water table elevation) in the saturated zone. 25
Figure 21: Average depth to water table in the WCW. 26
Figure 22: Average depth to water table in the fan area. 27
Figure 23: Average monthly recharge to saturated zone. 28
Figure 24: Average monthly recharge to the saturated zone in the fan area. 29
Figure 25: (a) Simulated depth to the water table and recharge at a point in the fan apex, shown in Figure 24. (b) Simulated depth to the water table and recharge at a point in the mountainous portion of the WCW, shown in Figure 23. 30
Figure 26. (a) Catchment averaged monthly simulated “recharge”. (b) Recharge as computed using a mass balance approach by subtracting actual evapotranspiration from infiltration. Black lines separate water years. 31
Figure 27. Water year water balance components. 33
Figure 28. Average monthly water balance components. 35
Figure 29: Annual average baseflow contributions from groundwater to Windermere Creek. 36
Figure 30: Average January baseflow from groundwater to Windermere Creek in the fan area. 37
Figure 31. Average April baseflow from groundwater to Windermere Creek in the fan area. 38
Figure 32. Average July baseflow from groundwater to Windermere Creek in the fan area. 39
Figure 33. Average October baseflow from groundwater to Windermere Creek in the fan area. 40
Figure 34: Precipitation and transfers to the SZ for (a) the 2019 wet WY and (b) the 2022 dry WY. 41
Figure 35: Depth to the water table in the fan area at the end of the 2019 wet WY(Sept 30). 42
Figure 36: Depth to the water table in the fan area at the end of the 2022 dry WY (September 30). 43
Figure 37: Windermere Creek gradient from the headwaters to the outlet at Windermere Lake. 44

Figure 38: Wetland located where the stream transitions from the mountain valley to the fan.. 45
Figure 39. Sediment thickness at the fan apex at the mountain front. 46
Figure 40. Day of the year when max SWE was attained at the Floe Lake station. 47

TABLES

Table 1: Land use class parameter inputs. 9
Table 2: Hydraulic properties for the main geological layers in the WCW model. 17
Table 3: Hydraulic properties for the geological lenses in the WCW model.. 17
Table 4: Unsaturated zone van Genuchten soil parameters. 19
Table 5: Final model parameters. 22
Table 6: Annual water balance components (mm/year) for individual water years over the last decade of the simulation period (2013 to 2023). 32
Table 7: Monthly average water balance components (mm/month) over the last decade of the simulation period (2013 to 2023). 34

1. INTRODUCTION

Sustainable water resource management and aquatic habitat protection/restoration measures in the face of climate change require good understanding of climatic and geologic controls on water movement through the landscape at the catchment scale. Of critical importance to long term planning and management in southern B.C. is information on groundwater recharge and discharge in alluvial fan aquifers, valley-bottom features under conflicting pressures between human use (i.e., domestic and irrigation water supply) and ecosystems (i.e., flows for fish).

This study focuses on exploring the seasonal and interannual groundwater dynamics and connectivity with surface water in Windermere Creek Watershed in response to concerns about groundwater sustainability in the fan area. In 2018, local residents reported that some domestic water supply wells in the upper part of the Windermere Creek fan (Windermere Loop Road area) had gone dry in recent years, leading to concerns about recharge sources and the sustainability of groundwater. In addition, local plans for fish habitat restoration in Windermere Creek, especially for the at-risk Westslope Cutthroat Trout, requires information about the connectivity between the creek and unconfined aquifer. Modelling spatial and temporal patterns in groundwater recharge and discharge is the starting point to addressing these concerns and knowledge gaps.

In response to the issue surrounding declining groundwater levels, Living Lakes Canada installed groundwater level monitoring equipment in two unused water supply wells along Windermere Loop Road in October 2018. Living Lakes Canada retained GW Solutions to develop a preliminary 3D hydrogeological conceptual model of the Windermere Loop Road area to help characterize the groundwater system. In 2021, GW Solutions was retained by Living Lakes Canada to update the 3D hydrogeological conceptual model to further characterize the groundwater system within the alluvial fan. Specifically, the 3D hydrogeological conceptual model was updated to 1) better understand the aquifer/aquitard system, 2) identify surface water and groundwater interaction zones along Windermere Creek, 3) identify potential sources of recharge to the aquifer, and 4) interpret available groundwater level data (GW Solutions, 2021). The 3D hydrogeological conceptual model was developed in Leapfrog Geo (Sequent 2022). High resolution LiDAR data were used to define the surface topography.

This study builds on an existing 3D hydrostratigraphic model of the alluvial fan (GW Solutions, 2021) commissioned by Living Lakes Canada. The main purpose of this study is to quantify the water balance for the Windermere Creek Watershed, identify recharge and discharge areas and where exchanges between surface water and groundwater occur, and explore the seasonal/interannual variability in these processes. The objectives were three-fold:

1. Construct an integrated hydrological model of the catchment;
2. Quantify the interannual and seasonal water balance for the catchment based on historical climate data; and
3. Identify patterns of recharge and discharge in the catchment, where exchanges between surface water and groundwater occur, and the contribution of groundwater to stream baseflow.

2. CATCHMENT SCALE INTEGRATED HYDROLOGICAL MODEL

2.1 Overview of the Modelling Software

MIKE SHE (Danish Hydraulic Institute (DHI), 2022) was selected for modelling the hydrologic processes within the Windermere Creek Watershed. MIKE SHE has been used in several watershed studies across B.C. to explore various aspects of the hydrological cycle (Voeckler et al. 2014; Foster and Allen 2015; Allen and Nott 2021; Dierauer et al. 2021). Unlike surface hydrological models, MIKE SHE is a fully integrated modelling package that can effectively simulate groundwater-surface water interactions. MIKE SHE is a deterministic and distributed modelling system that uses finite difference representations in mass and energy and measured empirical relationships to simulate aspects of the hydrologic cycle. The finite difference method uses a network of grid squares to represent the spatial variability of the land surface. The vertical discretization of the model domain is completed through the integration of unsaturated and saturated zone layers.

At its core is a framework of modules that are used to simulate the following processes: interception and evaporation, overland flow, unsaturated zone flow, and saturated zone flow. Rivers, lakes, and other channels are simulated in the one-dimensional model, MIKE HYDRO River, which is coupled directly to the MIKE SHE model. A brief summary of the modules is discussed below.

- The interception and evaporation module computes the actual evaporation (AET) from an area using user-defined potential evaporation (PET), using the Kristensen and Jensen (1975) model. This model requires vegetation dependent parameters such as leaf area index (LAI), rooting depth, and an interception parameter to calculate AET.
- Unsaturated flow in MIKE SHE is calculated in one dimension (1D), vertically. Three options are available for simulating flow in the unsaturated zone. The Gravity Flow method was used in this study. This method is not as computationally intensive as the 1D Richards' Equation method but is best suited for larger scale regional models and investigating recharge to groundwater based on precipitation and actual ET.
- The overland flow component simulates runoff when infiltration capacity of the soil is exceeded, when groundwater discharges to the surface, or when streams flood their banks. In this study, the flow solution utilized the diffusive wave approximation of the Saint-Venant equation, whereby topography and the Manning's M coefficient control the direction and rate of runoff, respectively.
- The saturated zone flow component in MIKE SHE is three dimensional (3D) and is based on Darcy's equation. Boundary conditions (such as fixed head, zero flux, gradient, and specified flux) are options which control the flow of groundwater within the model and attempt to mimic real world conditions. The subsurface was modelled as layers and lenses, with representative hydraulic properties assigned.
- MIKE HYDRO River simulates the routing of water in rivers and lakes. The rivers module is comprised of four main components: the river network, river cross-sections, boundary conditions, and hydrodynamic parameters. MIKE HYDRO River solves channel flow using the 1D Saint-Venant equation based on the dynamic wave formulation (Thompson et al., 2004).

MIKE SHE and MIKE HYDRO River are coupled using river links (h-points). During a simulation, the amount of water entering or exiting the linking cells is calculated based on Darcy's equation. Lateral inflows and outflow from overland flow as well as river-aquifer exchanges are completed for each computational time step (DHI, 2022).

2.2 Topography

The Windermere Creek Watershed (WCW) is a small 89.2 km^2 snowmelt-dominated mountain-to-valley catchment in southeastern B.C., itself being a small tributary of the Columbia River Basin in the Rocky Mountain Trench (Figure 1). Windermere Creek drains into Windermere Lake, which is a widening of the Columbia River. The WCW has an elevation range from a minimum of 800 masl at the lake, to a peak of 2,633 masl in the headwaters.

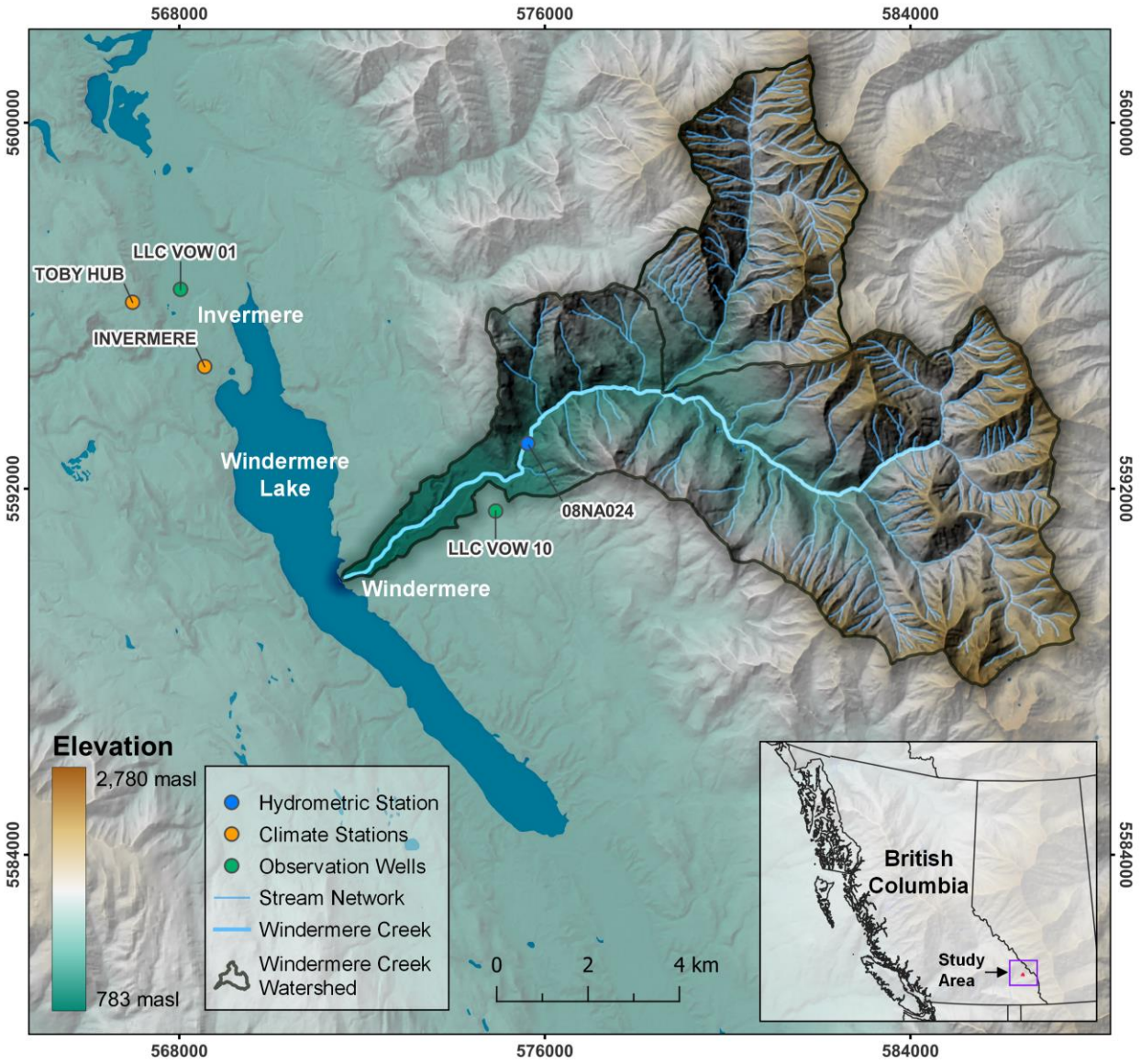

Figure 1: Windermere Creek Watershed (WCW). The locations of the hydrometric station (08NA024), two climate stations (TOBY HUB and Invermere) and Living Lakes Canada observation wells (LLC VOW 01 and LLC VOW 10) are shown.

Two digital elevation models (DEMs) were used to represent topography within the study area, and as the model surface input. For the fan area, a LiDAR-derived 1 m resolution DEM (tile 082j041) was used, from the provincial LidarBC repository (GeoBC, 2021). LiDAR data was chosen because of the typically higher vertical elevation accuracy, important for topographic feature representation. The 1 m LiDAR-derived DEM has a mean vertical error (RMSE) of 13.2 cm. The remainder of the catchment used a satellite derived ~16 m resolution DEM (tiles 082j12w and 082j05w) from the BC CDED DEM product (GeoBC, 2020). All DEMs, and concurrent spatial data, were reprojected to the UTM 11N NAD83 (EPSG: 26911) coordinate system. The workflow for processing the DEMs is shown in Figure 2.

The 1 m LiDAR DEM was merged with the 16 m CDED DEM to capture more detailed and complex topography of the alluvial fan as illustrated in Figure 3. The LiDAR DEM was inserted into a cut-out of the CDED DEM, with a 20 m overlap around the edges, which was then blended using a feathering technique. This ensured a smooth transition between DEM products that vary in spatial resolution and vertical accuracy. The merged DEM, resampled to 10 m for model input, was then hydroconditioned using a least-cost breach depressions algorithm (Lindsay and Dhun, 2015) from WhiteboxTools (Lindsay, 2016). DEM hydroconditioning is a crucial pre-processing step, especially for use in hydrological models, necessary in ensuring adequate overland flow across complex topography. The conditioning process involves removing or filling surface obstructions and depressions, respectively, that would cause significant impoundment of surface water. The existing stream network was acceptable, thus, no custom stream network extraction was performed on the hydroconditioned DEM.

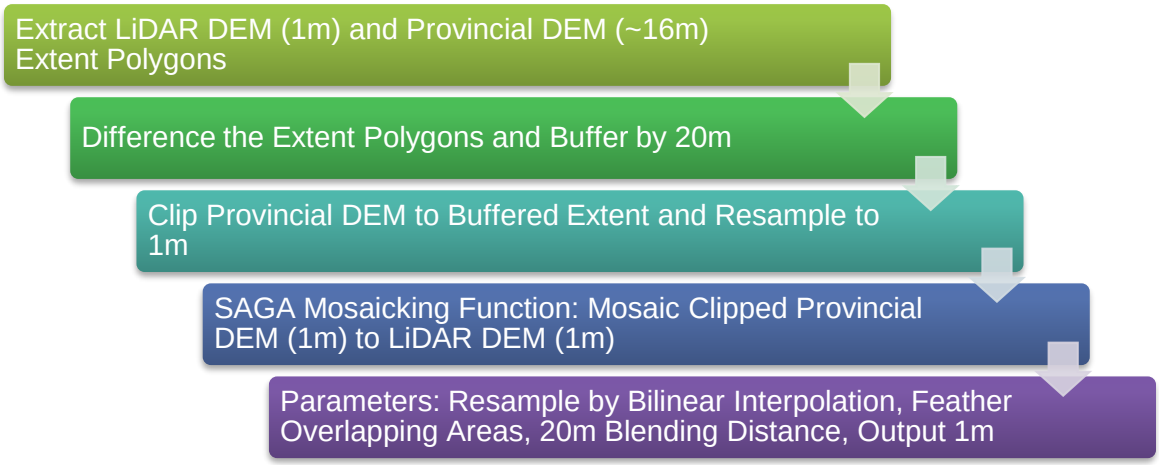

Figure 2: Summary of DEM mosaicking workflow in QGIS for joining a high- and low-resolution DEM.

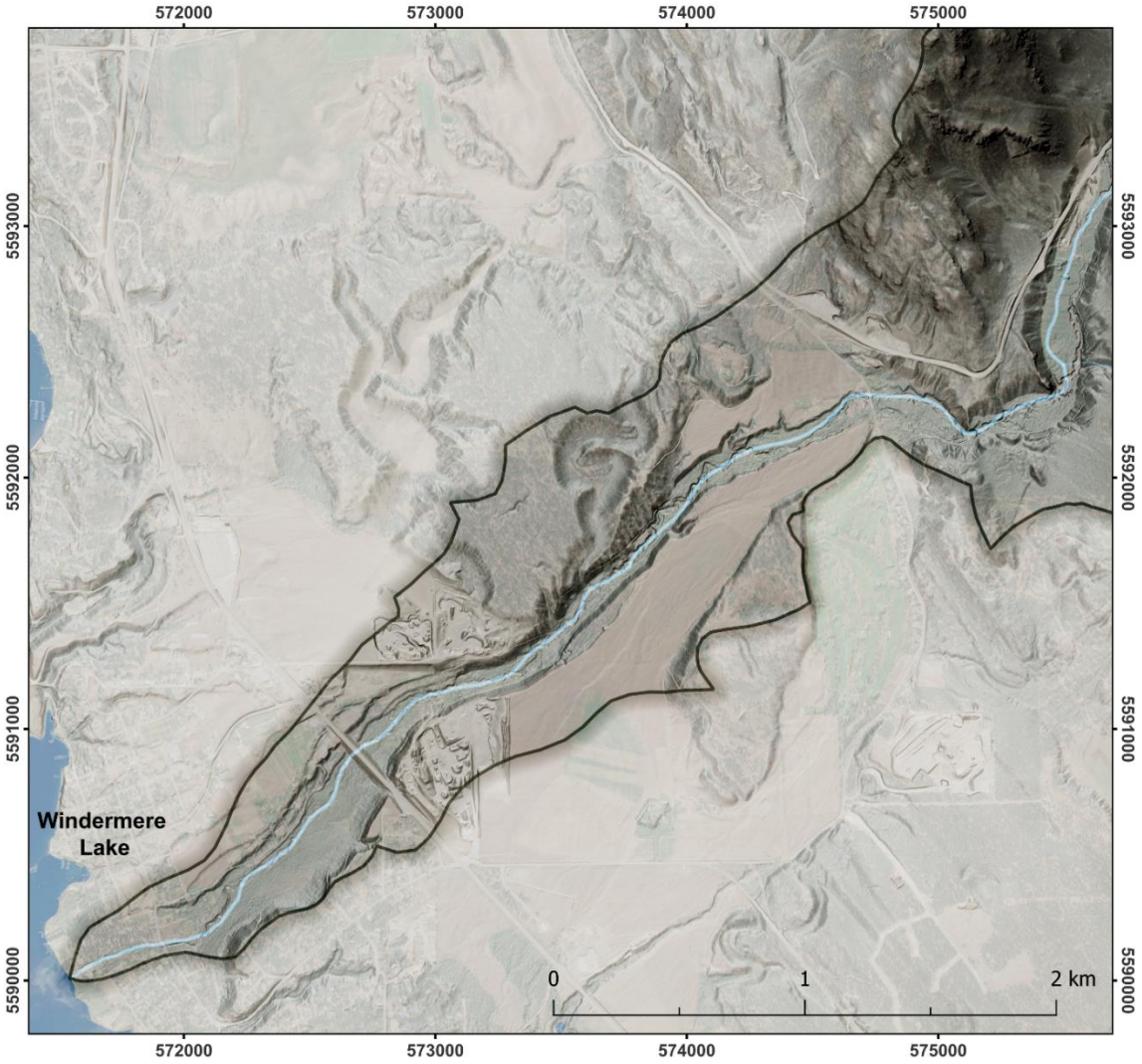

Figure 3: Complex topography of the WCW fan visible using the LiDAR-derived 1m DEM. The stream valley is deeply incised into the glacial sediments.

2.3 Climate and Weather

Windermere climate is classified as Dfb (Humid Continental, mild summers, wet all year) in the Köppen classification scheme. The 1991 to 2020 climate normals (Figure 4) are based on climate data from the Toby Climate Station (FLNRORD 417) in Invermere, about 5 km northeast of Windermere. This climate station is located at an elevation of 894 masl. Because of the large range in elevation across the WCW, valley-bottom climate might be well represented by this climate station; however, climate varies with increasing elevation. The WCW receives an average of 315 mm of precipitation per year, of which approximately 22% falls as snow. Precipitation peaks in June and decreases gradually until reaching a minimum in February. Mean monthly temperatures range from -7.0 °C in December to 18.8 °C in July. Minimum monthly temperatures are below freezing from October to April during which most precipitation is thought to fall as snow, especially at higher elevations. The mean daily temperature trend over more than the last 50 years (1968 to 2022) is +0.46 °C ($p = 0.0013$) while the maximum daily temperature trend is +3.26 °C ($p = 0.0088$) and the minimum daily temperature trend is -1.84 °C ($p = 0.0075$). Temperatures have risen by nearly half a degree Celsius in the region of the WCW.

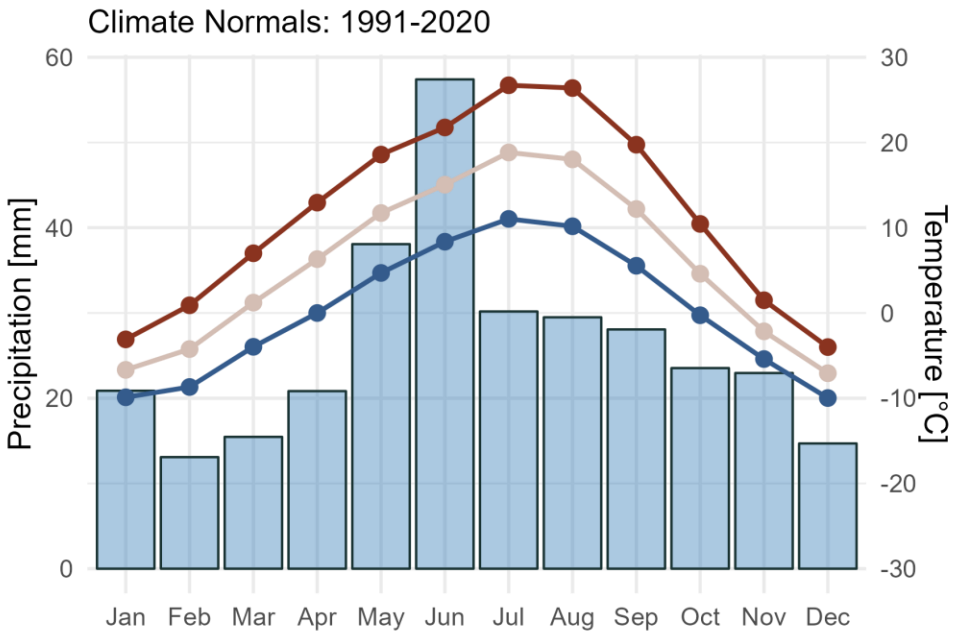

Figure 4: Climate normals (1991-2020) for the Toby Climate Station (FLNRORD 417) in Invermere. Maximum monthly temperatures are shown in red, mean monthly temperatures in beige, and minimum monthly temperatures in blue.

The CanSWE database (Vionnet et al., 2021) has a snow pillow station 53 km east of the WCW (Three Isle Lake, operated by the Government of Alberta), which has recorded snow water equivalent (SWE) for several decades (Figure 5a). BC Hydro operates an automated snow weather station at Floe Lake (BC Hydro 2C14P), 67 km north of the WCW, which has continuously recorded SWE since 1993 (Figure 5b). Magnitudes of SWE at these stations are unlikely to be representative of the WCW but are of interest regarding the timing of snowpack accumulation and melt. SWE tends to peak by the end of April, when temperatures begin to rise above freezing. By mid to late July, there is likely no snowpack in the WCW. The snowpack likely starts to accumulate in October once minimum daily temperatures drop below freezing at higher elevations.

The MIKE SHE model is forced with weather data, requiring time series data for precipitation, air temperature and reference (or potential) evapotranspiration (ET). Note that reference ET is not equivalent to actual ET; actual ET is calculated by MIKE SHE (see Section 2.4). Weather data may be applied uniformly across the watershed using data from a single climate station or distributed across the watershed, either as climate zones associated with two or more climate stations or as gridded data. For this project, both temperature and precipitation from the Toby Climate Station (FLNRORD 417) in Invermere were corrected for elevation by applying lapse rates.

Daily total precipitation and mean temperature from the Toby Climate Station for 1968-2022 were input to MIKE SHE. Reference ET was computed using the Penman-Monteith FAO56 method (Allen et al., 1998) implemented by Zotarelli et al. (2015). Shortwave radiation, wind speed, and relative humidity needed to calculate ET were sourced from the NASA Power dataset (NASA POWER 2023). The MIKE SHE default temperature lapse rate of -0.649 °C/100 m elevation gain was used initially and adjusted during calibration. When raining, the temperature lapse rate was -0.3 °C/100 m, the default value used by MIKE SHE.

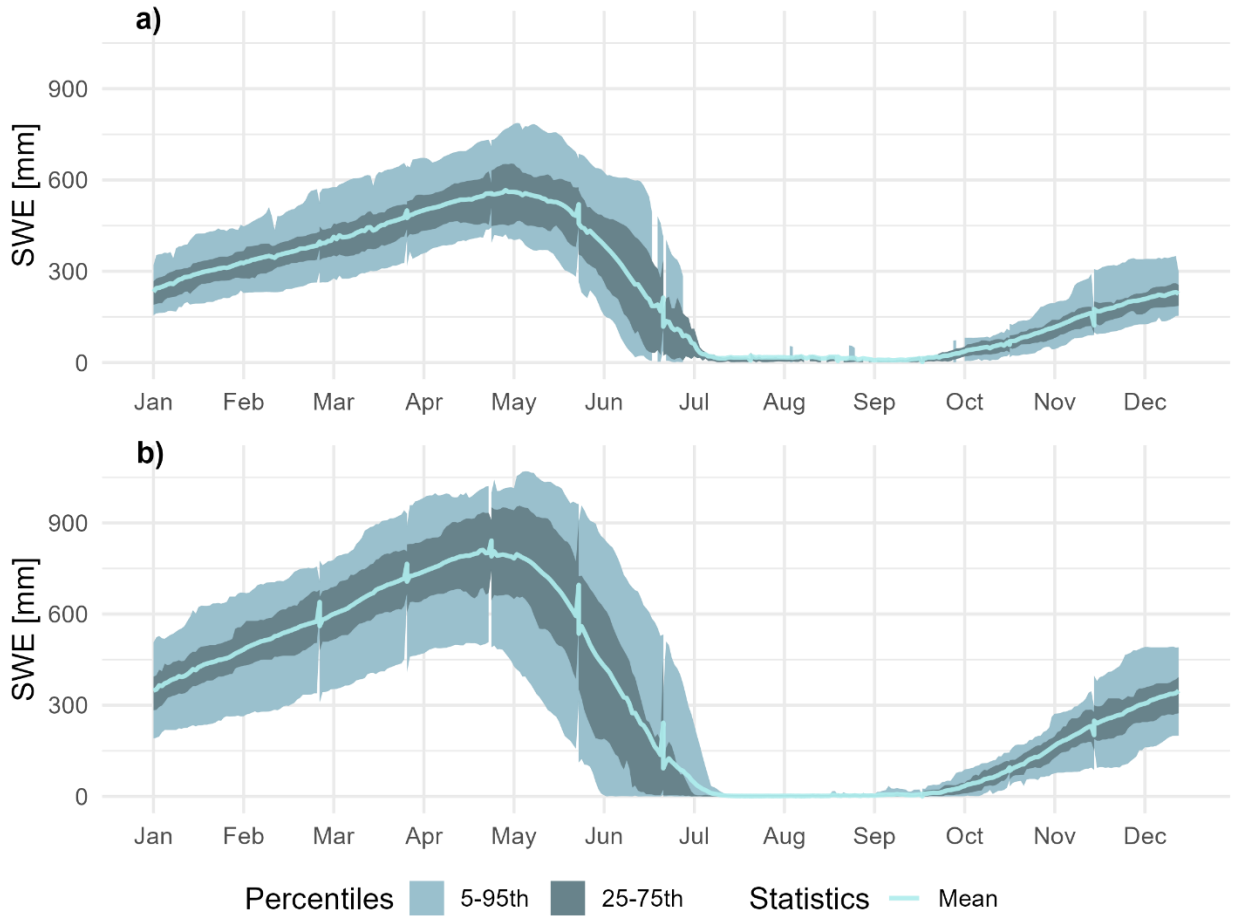

Figure 5: Mean daily snow water equivalent (SWE) from a) the Three Isle Lake snow pillow station 53 km east of Windermere (operated 1985-2022, elevation: 2160 masl), and b) the Floe Lake snow weather station 67 km north of Windermere (operated 1992-2022, elevation: 2090 masl).

Snowmelt was simulated using the degree-day method, using a uniform degree-day coefficient of 2 mm/°C/day, and a maximum wet snow fraction in snow storage of 0.3. Thermal melting for snowmelt was included, using the default value of 0.5 $°C^{-1}$ for the melt coefficient of the thermal energy in rain. All other snowmelt parameters were left as default values (see Section 2.10). A precipitation lapse rate of 10 %/100 m elevation gain was initially used and adjusted during calibration (see Section 2.10) to allow for more snow to accumulate in the colder mountain tops.

2.4 Land Use and Vegetation

An important input parameter required to calculate actual evapotranspiration (AET) is leaf area index (LAI), a quantifiable measurement of vegetation density within the watershed. MIKE SHE has capability of modelling uniform or distributed, and static or dynamic changes in land use and vegetation. For the WCW, distributed land use classes were set as constant (static) throughout the simulation. The limitation of using static land use was that seasonal variation in LAI was not represented (Rautiainen et al., 2012). Further refinements of the model could explore seasonally varying LAI. Land use classes were derived from the 2015 Land Cover of Canada dataset (Natural Resources Canada, 2019), available at a 30 m resolution (Figure 6). LAI values from Chen et al. (2002) were used (Table 1). Water bodies, urban areas (largely paved) and areas covered by snow and ice were assigned a LAI of 0 (Table 1). The

vegetation module in MIKE SHE also contains ET parameters, which can be altered based on site specific data. The parameters include canopy interception (default value of 0.05 mm), which needs to be exceeded before stem flow and ground infiltration can occur, and empirical coefficients C1, C2, and C3, which relate to the Kristensen and Jensen equation that MIKE SHE uses to calculate actual transpiration and soil evaporation. Coefficients C1 and C2 are plant dependent and influence the distribution between soil evaporation and transpiration. These parameters were set to the default values of 0.3 and 0.2 mm/d, respectively. Coefficient C3 is soil dependent and controls the release of water at certain matrix potentials and root densities; this parameter was set to the default value of 20 mm/day. The final ET parameter is the AROOT parameter value, which was assigned as the default of 0.25 m^{-1}. This parameter controls the fraction of ET extracted as a function of depth, as larger values have a greater range of ET, and approaches uniformity as the value nears 0. The biome-averaged rooting depths from Yang et al. (2016) for similar land use classes were used (Table 1). Barren areas, water bodies, urban areas and areas covered by snow and ice were assigned a rooting depth of 0 m.

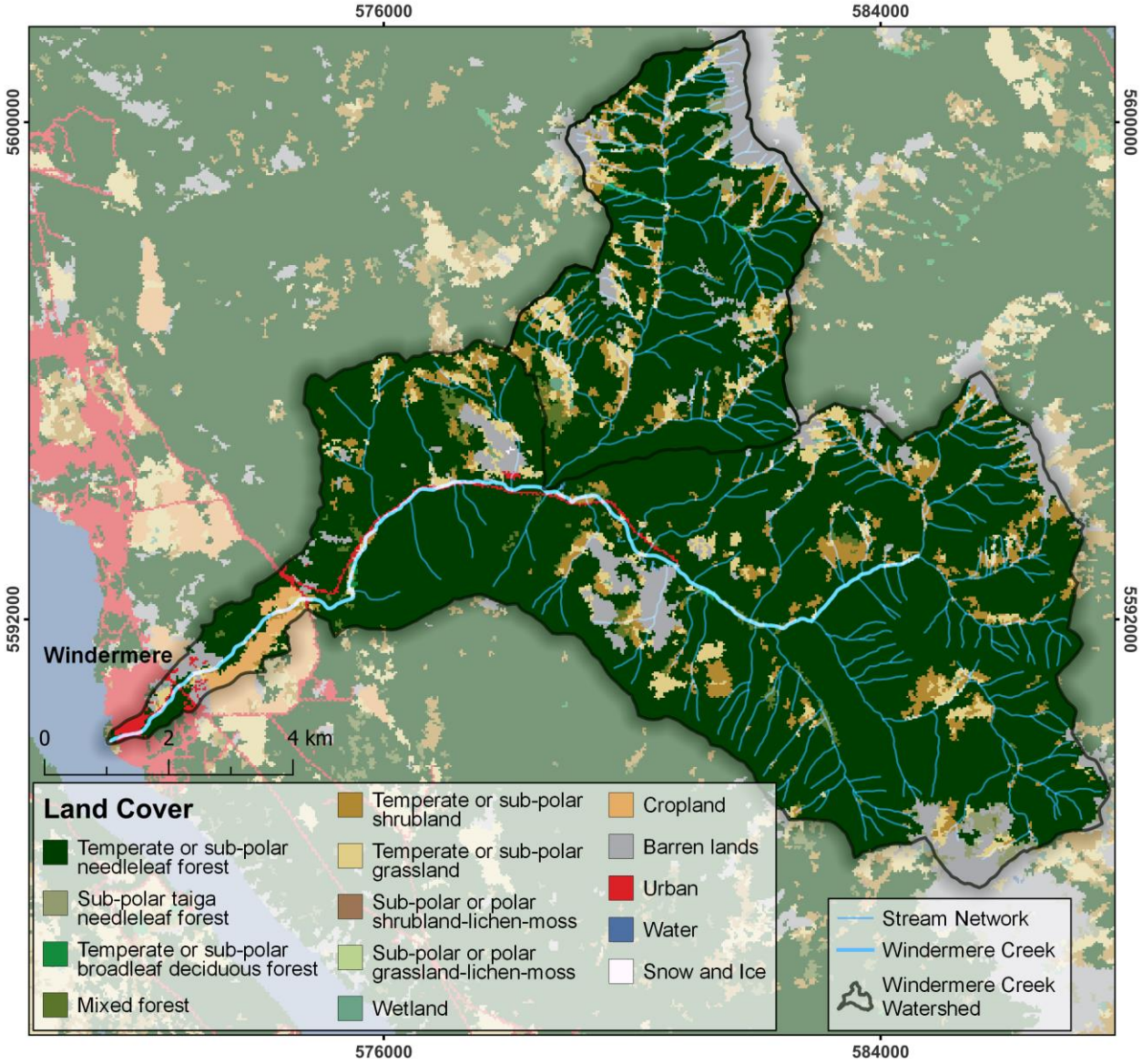

Figure 6: 2015 Land Cover of Canada classes within the study area (Natural Resources Canada, 2019).

Table 1: Land use class parameter inputs. Leaf area index (LAI) estimates are from Chen et al. (2002). Rooting depth estimates are from Yang et al. (2016).

Land Use Class	LAI [-]	Rooting Depth [mm]
Temperate or sub-polar needleleaf forest	2.83	430
Sub-polar taiga needleleaf forest	2.83	430
Temperate or sub-polar broadleaf deciduous forest	3.99	1070
Mixed forest	0.54	3060
Temperate or sub-polar shrubland	1.21	370
Temperate or sub-polar grassland	0.61	510
Sub-polar or polar shrubland-lichen-moss	1.21	370
Sub-polar or polar grassland-lichen-moss	0.61	510
Wetland	0.45	510
Cropland	1.14	550
Barren lands	0.45	0
Urban	0	0
Water	0	0
Snow and Ice	0	0

2.5 Overland Flow

Overland flow is defined as the portion of runoff that occurs as sheet flow. If rainfall exceeds the infiltration capacity of the soil, water will move horizontally across the surface, routed by surface topography, at a rate calculated in MIKE SHE using the diffusive wave approximation. The resistance to overland flow is controlled by the "roughness" of the land surface, which can be inferred from land use/cover maps. Within MIKE SHE, the Manning's M coefficient (reciprocal of Manning's n) controls the amount of friction and the velocity at which water can move horizontally over land. For the WCW model, Manning's M was set to 30 $m^{1/3}/s$ (equivalently 0.033 $s/m^{1/3}$ for Manning's n). Generally, lower values of Manning's M are used for overland flow compared to channel flow (see Section 2.6 for channel flow). Further refinements of the model explored different ranges of Manning's M, but it was ultimately left at 30 $m^{1/3}/s$. Detention storage, which is the depth of ponded water that must be exceeded for overland flow initiation, was set to 1 mm.

2.6 Streamflow

The WCW is currently ungauged but had a stream gauge at the foothills (see Figure 1) in continuous daily operation from 1959 to 1979 by Environment and Climate Change Canada (ECCC) (Figure 7). Increasing temperatures at the end of April initiate snow melt at low and mid- elevations, causing a rapid rise in streamflow. Streamflow peaks by mid-June. Streamflow recession reaches a minimum by the end of April. The hydrograph recession is supplemented during the rainy summer and fall seasons. Monthly timings of flow over the operational period of the gauge are shown in Figure 8.

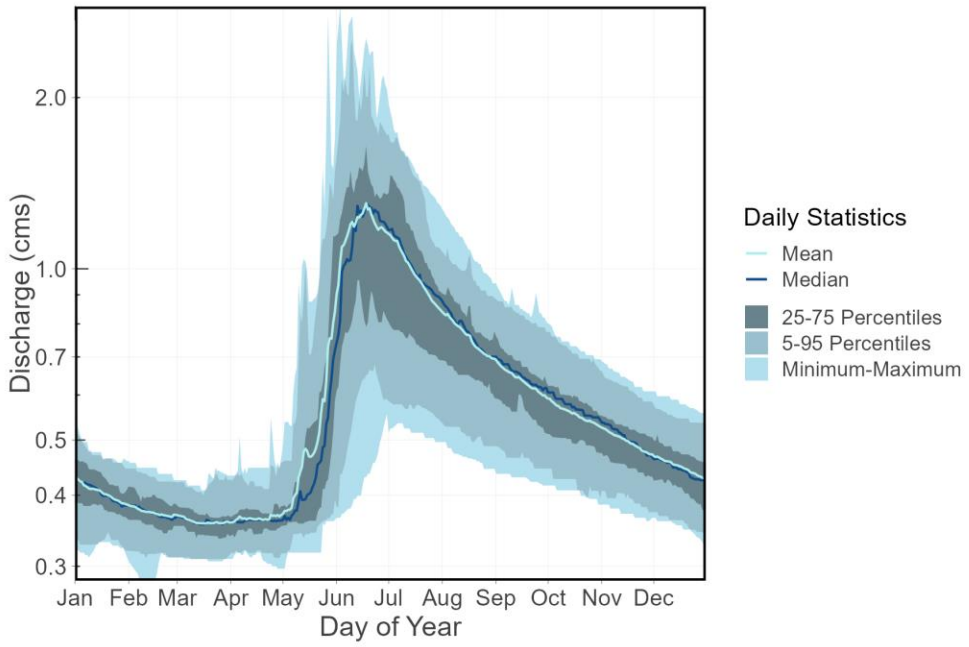

Figure 7: Windermere Creek hydrograph (ECCC Station 08NA024) showing daily statistics for the period 1959-1979. Stream discharge is shown in cubic metres per second (cms).

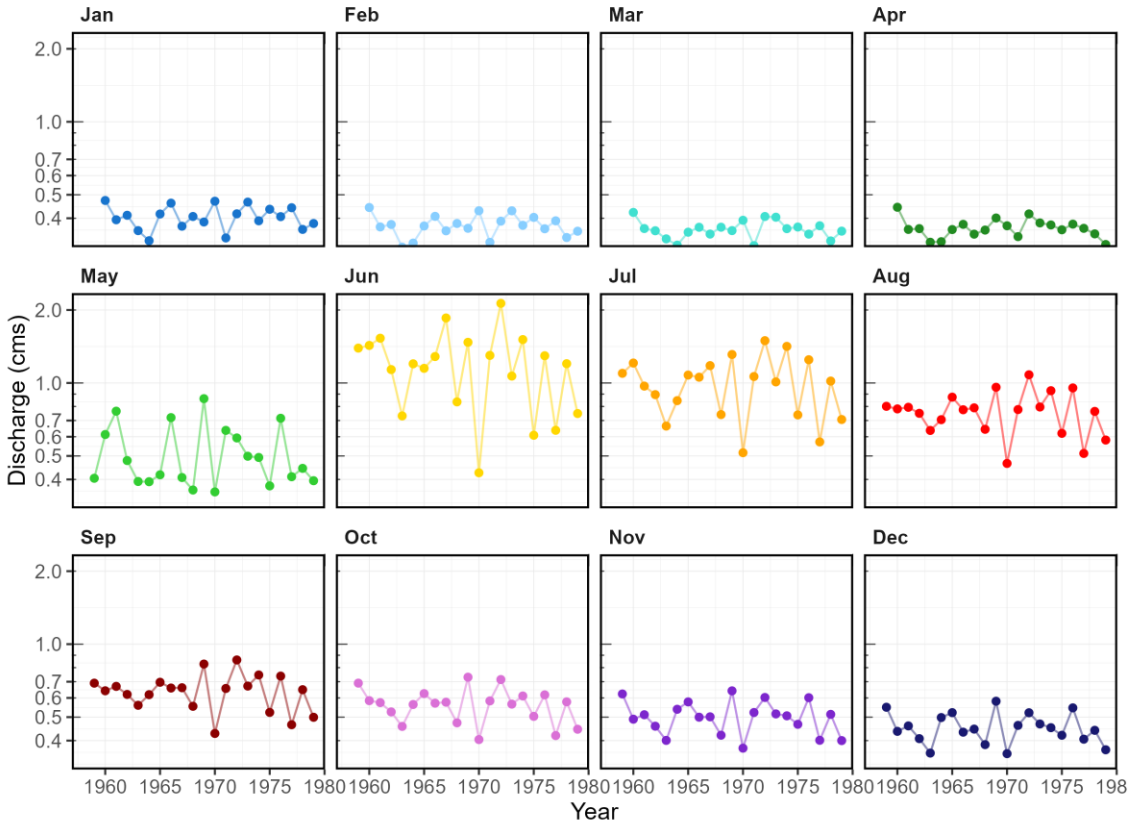

Figure 8: Windermere Creek monthly flows (ECCC Station 08NA024) from 1959 to 1979. Discharge is shown on a log scale in cubic metres per second (cms).

River routing must first be run in a separate module, MIKE HYDRO River, which is then coupled to the MIKE SHE model. The MIKE River module is a framework for running one-dimensional river routing, allowing for an interface between overland flow and groundwater exchanges in MIKE SHE. MIKE River requires four main components (Figure 9) 1) a stream network, 2) stream cross-sections, 3) boundary conditions, and 4) bed roughness.

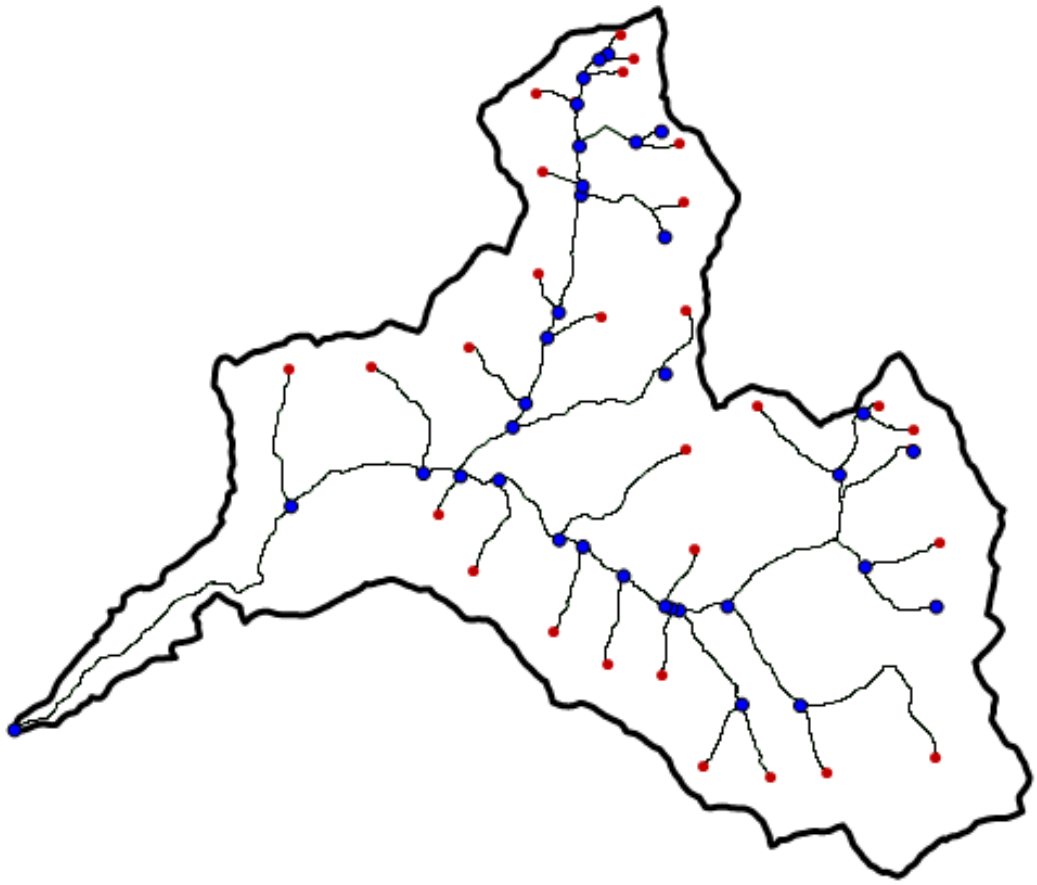

Figure 9: WCW MIKE HYDRO River stream network. Branch connection nodes are shown in blue, and boundary nodes in red.

The stream network used within the WCW was clipped from the BC Freshwater Atlas (GeoBC, 2023). Nine manually surveyed cross-sections were collected by Natasha Neumann and Carol Luttmer on October 5-6, 2022 [see appended Excel spreadsheet]. Additional cross-sections were generated and mapped in MIKE HYDRO, spaced 25 m apart and made 25 m wide. Bed resistance (Manning's M) was set to a global value of 20 $m^{1/3}/s$ (or equivalently 0.05 $s/m^{1/3}$ for Manning's n). Two boundaries were applied: the upstream boundary at the headwater was an open discharge constant flow of $1x10^{-5}$ m^3/s. The downstream boundary was a constant water level (stage) boundary held at the mean lake level of 802 masl. The lake level was held constant throughout the simulation due to lack of information of time-varying lake stage.

Finally, the MIKE River model was coupled to MIKE SHE via branch couplings. River-aquifer exchanges were controlled independently for each branch through a conductance (in m^2/day) exchange method and associated leakage coefficients. The default aquifer and riverbed conductance exchange method was used, wherein the exchange of water is a function of both the aquifer hydraulic conductivity and the

river bed hydraulic conductivity. The riverbed conductance is controlled through a leakage coefficient (in day^{-1}), which was initially left to the default of $1x10^{-8}$ day^{-1} but adjusted to $1x10^{-5}$ following model calibration. Therefore, the volumetric exchange between the river and the saturated zone was mediated by the leakage of the riverbed lining. A larger leakage coefficient will result in a larger conductance, allowing for a less restricted exchange (i.e., there is less resistance to exchange flows between the aquifer and the stream).

2.7 Geology and Groundwater

The underlying bedrock of the WCW is quite complex, containing a faulted melange of carbonates and lightly metamorphosed sedimentary rocks (Figure 10). The upstream portions of the WCW are predominantly dolomitic carbonates that are bisected by two major north-south oriented faults. The downstream valley sediments sit atop mudstones and shales, rather than the carbonates.

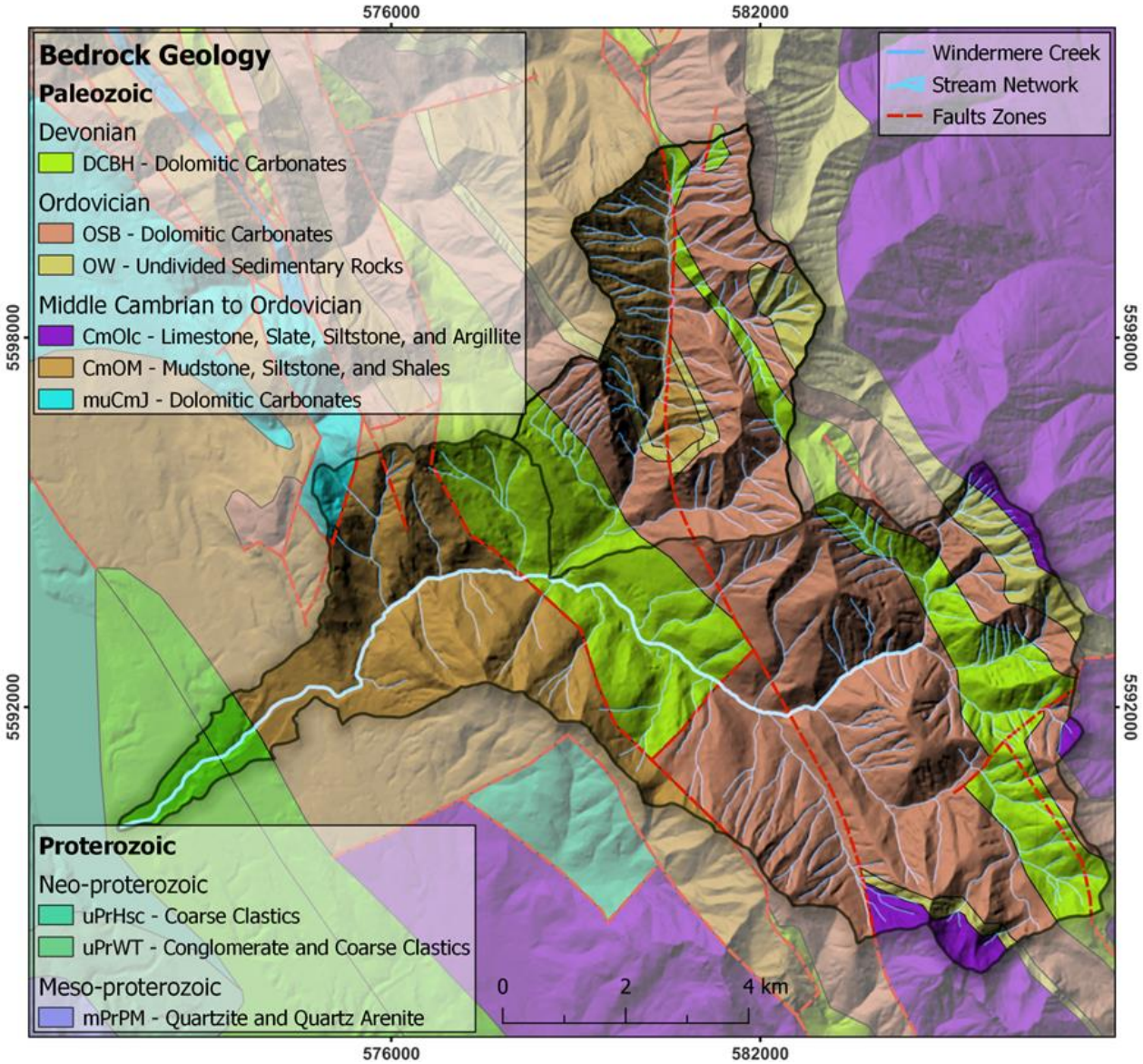

Figure 10: Bedrock geology of the WCW (B.C. Geological Survey (BCGS), 2019).

The subsurface geology within the valley (fan area) was modelled by GW Solutions Inc. (2021) using Leapfrog Geo 2022.1 (Seequent, 2022). This 3D conceptual model derived information on depth to bedrock as well as vertical and horizontal patterns in unconsolidated sediments from groundwater well drilling logs. Leapfrog Geo files were provided for this study for the purpose of representing the subsurface in the fan area. The reader is directed to the GW Solutions Inc. (2021) report for details on the development of the geological model in the fan area.

Sediment thickness is shown in Figure 11, which was derived in this study by subtracting the ground surface DEM from the bedrock DEM. The valley is extensively terraced with discrete plateaus with sediments thicknesses of over 200 m. Valley sediments generally range from a thickness of 50 to 150 m. Sediment cover in the mountainous areas in the northeast is quite thin, where bedrock is much closer to ground surface.

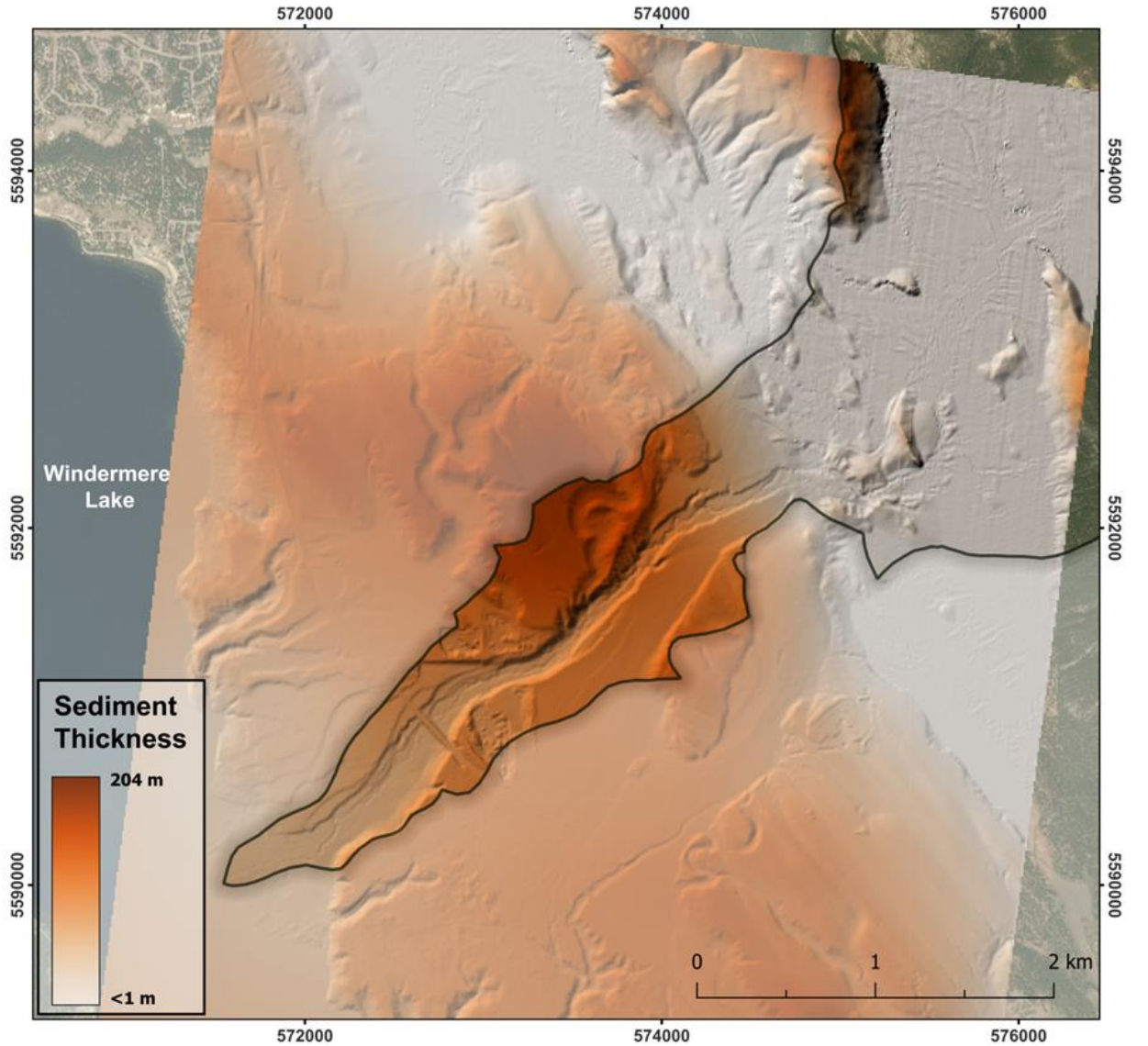

Figure 11: Sediment thickness in the WCW valley. Areas in grey have very thin sediment cover, especially in the mountainous areas to the northeast.

Based on the groundwater system described by GW Solutions Inc. (Figure 6; 2021) and the bedrock information, a conceptual hydrogeological model for the WCW is presented, summarizing all available geological information (Figure 12). The upstream mountainous area of the WCW is bedrock dominated with a thin veneer of alpine soils. The transition area from the mountain system to the valley contains of a sand and gravel aquifer system sitting atop a thick clay aquitard. Within this aquitard is a thin confined aquifer of limited extent. Based on hydrogeological studies in similar mountain regions, a weathered bedrock layer overlies fractured bedrock (Welch and Allen, 2014). Allen and Nott (2021) incorporated a weathered zone into a hydrological model of a small headwater catchment in the interior of B.C. and found that model calibration improved over a previous hydrological model for the same catchment that did not include a weathered zone (Voeckler et al., 2014).

To reduce model complexity in this study, no distinction is made between bedrock lithologic units, and none of the mapped faults are included. Unfortunately, there are no physical data, other than their mapped locations, to allow their distinction in the model. The hydraulic properties of the hydrogeological units are defined in Section 2.8.

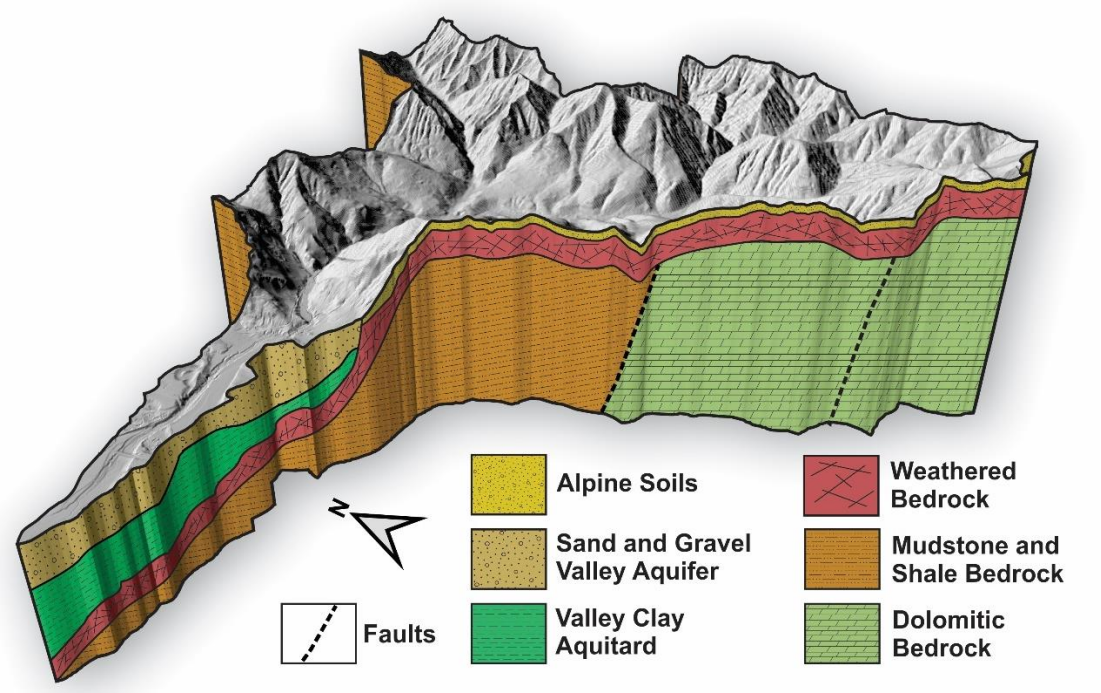

Figure 12: Geological conceptual model of the WCW.

Living Lakes Canada (LLC) operates a semi-active monitoring groundwater well in the main valley south of the WCW boundary (~500 m), named as Voluntary Observation Well (VOW) 10 (LLC 2023). This station has three years of data (2018 to 2021). VOW 10 corresponds to well 66814 in GWELLS (2023) and has been correlated to mapped aquifer 453, a confined glaciofluvial sand and gravel aquifer. This aquifer is quite thick and responds relatively quickly to the onset of snowmelt (Figure 13), suggesting that the aquifer may be semi-confined. For example, in 2020 snowmelt at the Floe Lake snow pillow station began on May 5th, indicating that melt was already occurring at mid-elevations; shortly afterwards, on May 27th, the groundwater level in VOW 10 reached its lowest point and began to rise in response to melt inputs. Although the snowpack was lower in 2019 compared to 2020, groundwater levels were higher. This suggests that summer and autumn rains in 2019 may have contributed additional recharge.

Although located in Invermere, VOW 01 offered insight into what was happening in the shallow subsurface (LLC, 2023) and which we correlated to mapped aquifer 603 (using nearby wells), an unconfined fluvial sand and gravel aquifer. This well was heavily influenced by both snowmelt and rainfall but does show an unusual winter rise, during a time which the snowpack is accumulating and precipitation is likely falling as snow (Figure 13). The unusual response at this well is possibly due to the influence of ice jams in the Toby Creek, a few hundred metres away, causing localised groundwater recharge (C. Luttmer, pers. comm., 2022).

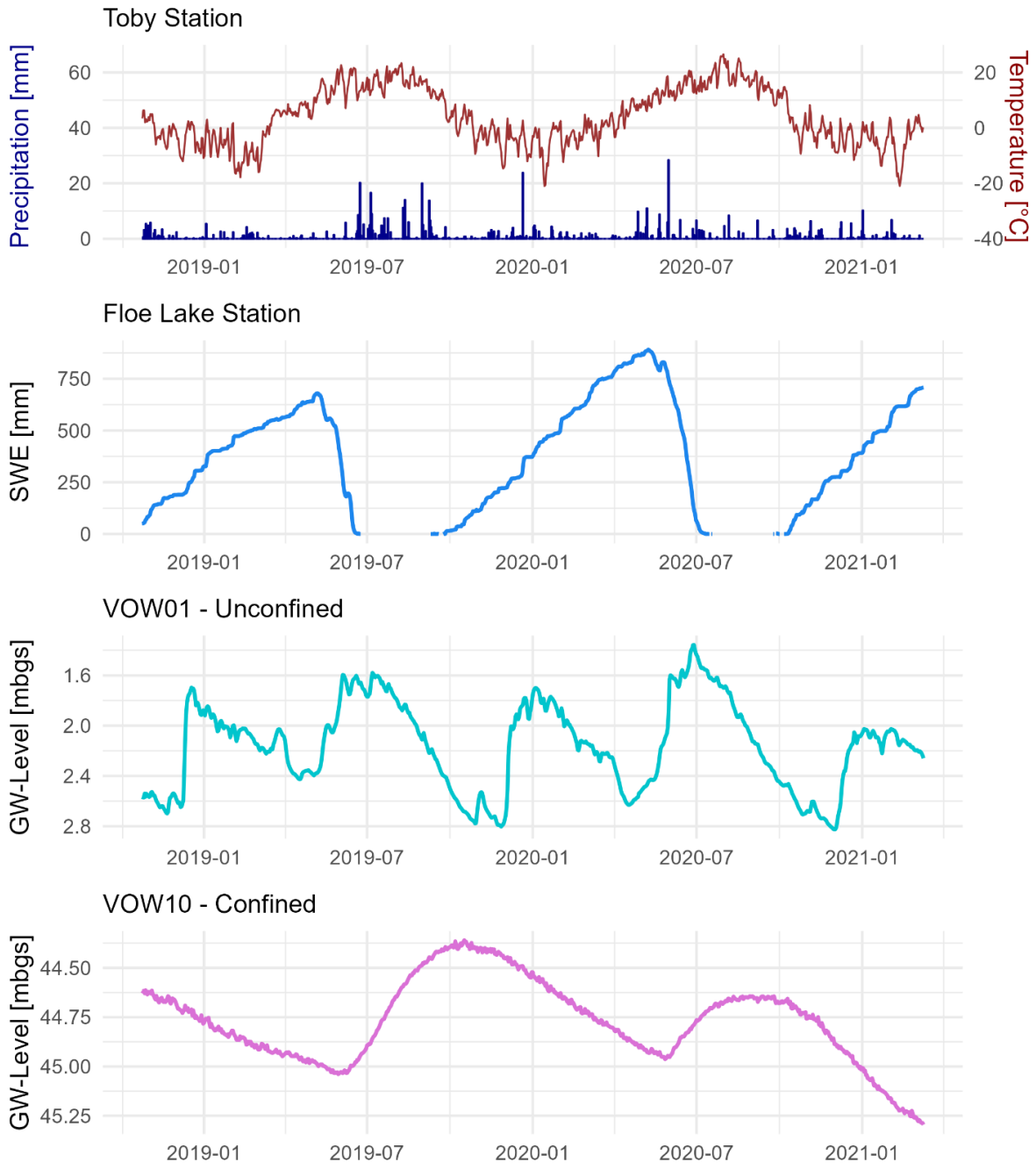

Figure 13: Meteorological and SWE data for 2018-2021 shown with both groundwater monitoring wells (see Figure 1 for station and well locations).

2.8 Model Structure and Parameterization

In MIKE SHE, the subsurface is divided into two zones: unsaturated and saturated. These two zones overlap so that water can transfer between them. The following subsections provide details on how these zones were represented.

2.8.1 Saturated Zone

In the saturated zone, MIKE SHE simulates groundwater flow using a 3D finite difference method, similar to MODFLOW. Hydrogeological units in the WCW were defined using a combination of geological layers and lenses (Figure 14), which were both discretized vertically into computational layers (explained below).

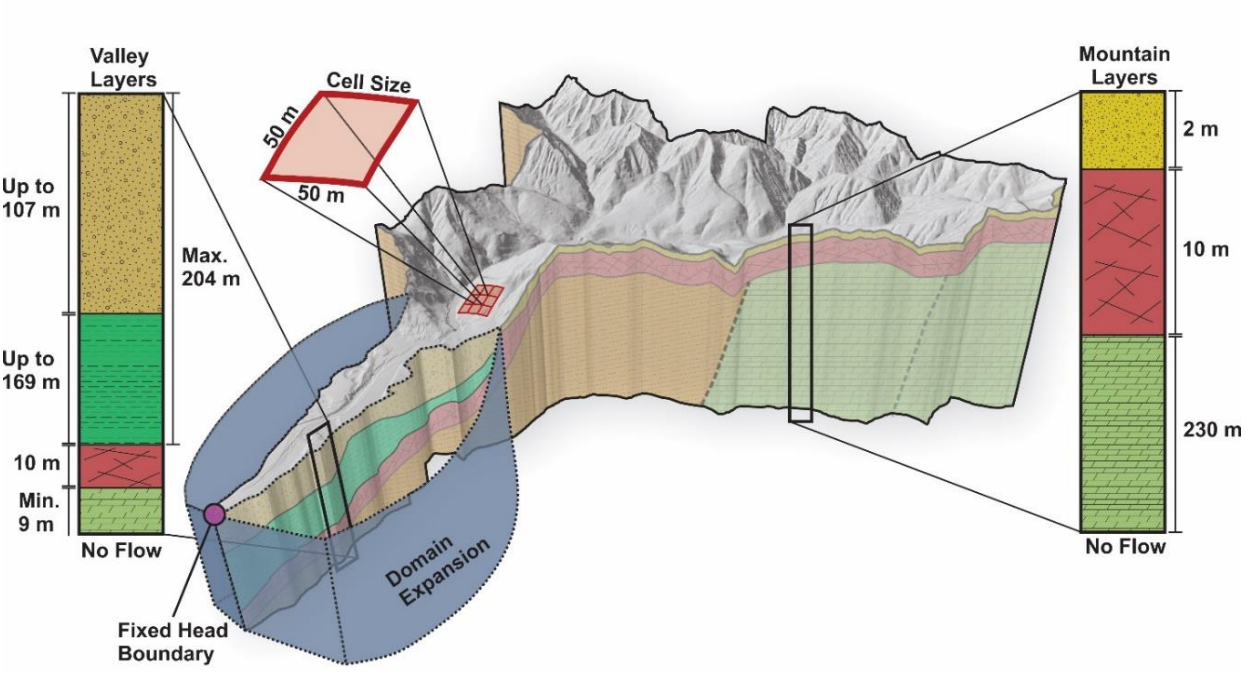

Figure 14: Hydrostratigraphic model structure for the WCW. The mountain layers in MIKE SHE consisted of soil & surficial sediments (gold), weathered bedrock (red) and bedrock (olive green). The valley layers consisted of unconsolidated unconfined aquifers (beige) and confined aquitards and aquifers (bright green), overlying weathered bedrock (red) and bedrock (olive green). The valley layers were defined as lenses in MIKE SHE, which overwrite geological layers (see Figure 15).

The entire saturated zone was first defined as being composed of three layers: surficial sediments, weathered bedrock and bedrock (Table 2). This simplified approach was used to represent the upland mountain areas of the WCW where sediment cover is likely to be minimal compared to that of the valley.

In the unconsolidated valley deposits, geological lenses were used to represent aquifer and aquitard units that were discontinuous, and thus could not be defined by a simple layering scheme. Geological lenses (as defined in MIKE SHE) overwrite geological layers. The inclusion of the lenses substitutes the simplistic three-layer definition of the mountain block. GW Solutions Inc. (2021) provided their Leapfrog Geo (Seequent, 2022) geological conceptual model of the WCW valley, which is composed of several units, named in Table 3. Each of the units top and bottom meshes were extracted from Leapfrog Geo and imported into MIKE SHE, defining aquifer and aquitard geological lenses. This is only applicable for

the fan area. These lenses effectively replace (overwrite) the geological layers that exist in the background. The unit names used by GW Solutions (2021) were adopted for consistency, and the lenses were superimposed over a generic Valley Fill unit to fill gaps that may have emerged in the extracted layers. Hydraulic properties for each unit was approximated based on dominant lithology (Table 3). Specific yield (Sy) values were obtained from Harter (2005) and specific storage (Ss) and hydraulic conductivity (K) were obtained from Kuang et al. (2020). Values for Sy, Ss and K for the weathered bedrock and bedrock are similar to those used by Allen and Nott (2021) for a catchment in the interior of B.C.

Table 2: Hydraulic properties for the main geological layers in the WCW model. Geological layers are overwritten by geological lenses in the valley fill (see Table 3). Unit names are colour coded by the Mountain Layers column shown in Figure 14.

Unit Name	Layer Thickness [m]	Horizontal K [m/s]	Vertical K [m/s]	Specific Yield Sy [-]	Specific Storage Ss [m^{-1}]
Surficial Sediments	2	$5.0x10^{-4}$	$5.0x10^{-4}$	0.25	$1.8x10^{-4}$
Weathered Bedrock	10	$3.2x10^{-6}$	$3.2x10^{-7}$	0.10	$8.6x10^{-7}$
Bedrock	230	$1.0x10^{-8}$	$5.0x10^{-9}$	0.01	$8.6x10^{-7}$

Table 3: Hydraulic properties for the geological lenses in the WCW model. Lens thicknesses are variable. Unit names are colour coded by the Valley Layers column in Figure 14. The Valley Fill unit is used as a filler to account for any gaps.

Unit Name (from GW Solutions (2021))	Dominant Material	Horizontal K [m/s]	Vertical K [m/s]	Specific Yield [-]	Specific Storage [m^{-1}]
Alluvial Fan (Unsaturated)	Sand and Gravel	$1.7x10^{-4}$	$1.7x10^{-5}$	0.25	$1.8x10^{-4}$
Upper Aquifer (Saturated)	Sand and Gravel	$5.8x10^{-5}$	$5.8x10^{-6}$	0.25	$1.8x10^{-4}$
Aquitard (Confining)	Clay and Silt	$9.3x10^{-7}$	$9.3x10^{-8}$	0.10	$7.7x10^{-4}$
Middle Aquifer (Confined)	Sand and Gravel	$2.3x10^{-5}$	$2.3x10^{-6}$	0.15	$4.7x10^{-5}$
Lower Aquifer (Confined)	Sand and Gravel	$2.3x10^{-5}$	$2.3x10^{-6}$	0.15	$4.7x10^{-5}$
Valley Fill (Alluvial Fan Material)	Sand	$1.7x10^{-4}$	$1.7x10^{-5}$	0.25	$1.8x10^{-4}$

In the main valley, the saturated zone was vertically discretized into 16 computational layers to capture vertical changes in the hydraulic conductivity distribution within the geological lenses (Figure 15). Computational layers 1 to 10 are each 10 m thick (100 m total thickness), while layers 11 to 15 are each 20 m thick (100 m total thickness), and layer 16 is 50 m thick. While increasing the number of computational layers results in a greater resolution of hydraulic conductivities, it significantly increases the computational run time of the entire model.

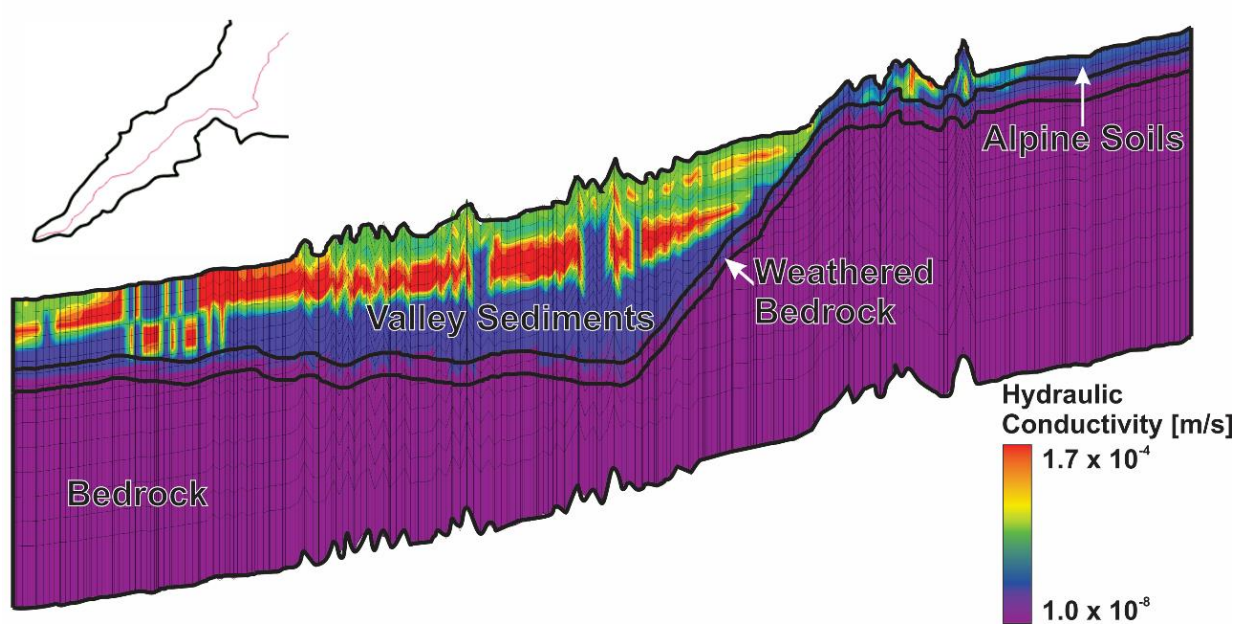

Figure 15: Computational layers and hydraulic conductivity distribution along a transect of the valley centre. The thin black lines are the computational layers.

2.8.2 Unsaturated Zone

The Gravity Flow method was used to model unsaturated flow. The method ignores capillary forces and is suitable when interested in the time varying recharge and not the dynamics in the unsaturated zone. The Green and Ampt model was also selected; it is an analytical solution to allow for the increased infiltration experienced in dry soils due to capillarity, such as may happen if the water table is deep. Infiltration is calculated based on the infiltration capacity of the soil and ponding occurs if the rainfall rate exceeds the infiltration capacity. This method is not as computationally intensive as the 1D Richards' Equation method but is best suited for coarser scale regional models and investigating recharge to groundwater based on precipitation and actual ET. The results best represent unsaturated flow under dynamic conditions at a coarse scale (DHI, 2022).

The unsaturated zone included soil, weathered bedrock and nonweathered bedrock. In the upland mountain area, the unsaturated zone profiles were 40 m thick, with vertical discretization as follows: soil = 0 to 2 m, weathered bedrock = 2 to 12 m, bedrock = 12 to 40m. In the valley area, the unsaturated profiles were 80 m thick, with vertical discretization as follows: surficial sediment = 0 to 40 m, weathered bedrock = 40 to 50 m, bedrock = 50 to 80 m.

Soil textural classes from the B.C. soil survey (B.C. SIFT, 2018) were used to delineate soil zones across the catchment (Figure 16). The soil moisture retention curve and the hydraulic conductivity function were determined using van Genuchten parameters, which were estimated for the different soil textural classes using tabulated literature values from Carsel and Parrish (1988) summarized in Shao and Irannejad (1999) (Table 4). Rock bulk densities were taken from Sharma (1997) and dry soil densities were taken from Linsley et al. (1982). Shao and Irannejad (1999) conclude that the van Genuchten formulation performed the best in soil moisture simulations in the context of hydrologic modelling.

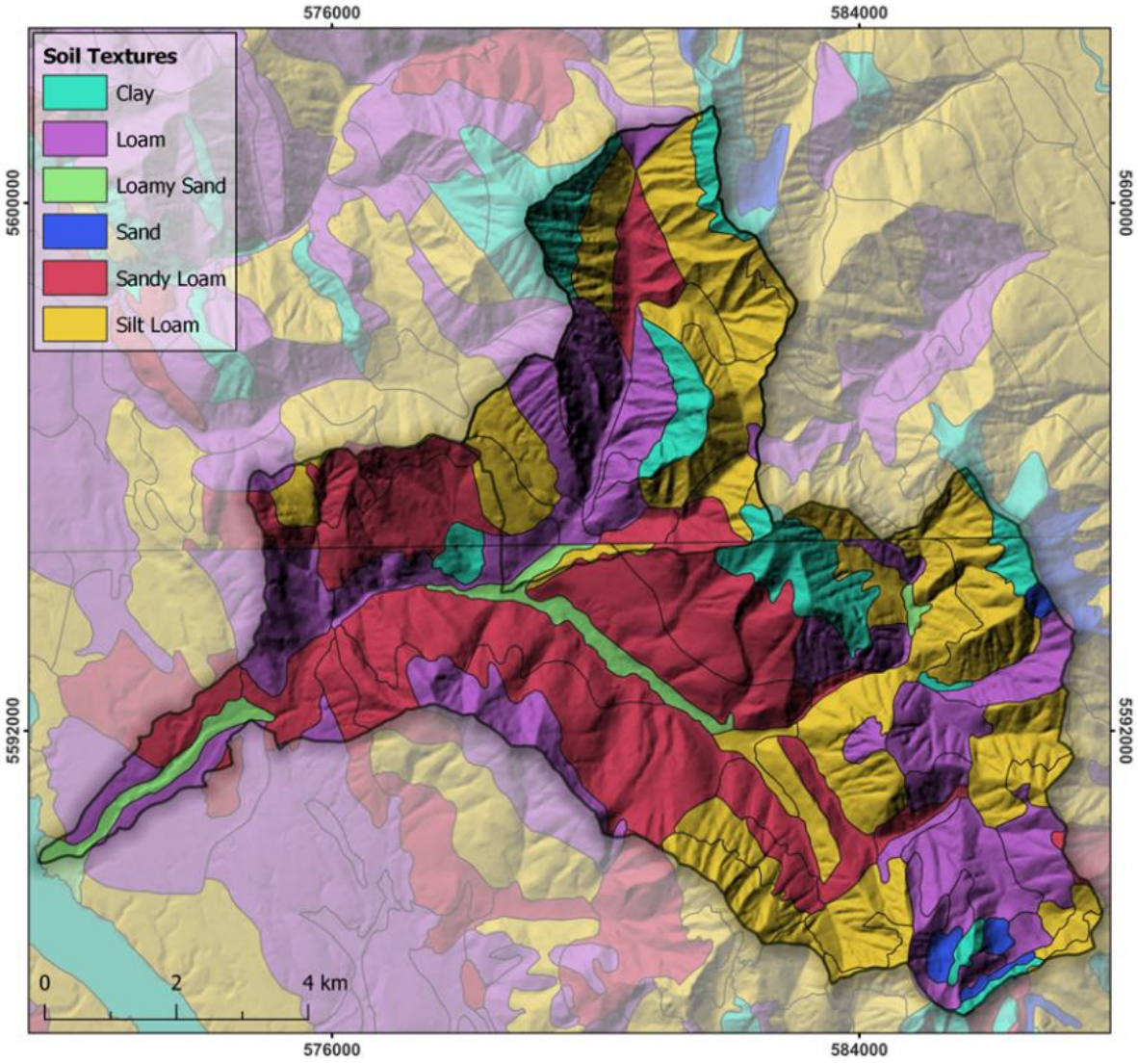

Figure 16: Soil textural classes from the BC soil survey (BC SIFT, 2018) that made up the unsaturated zone in the WCW.

Table 4: Unsaturated zone van Genuchten soil parameters.

Soil Texture	Dry Bulk Density (kg/m^3)	Saturated Moisture Content [θ_s]	Residual Moisture Content [θ_r]	α [cm^{-1}]	m [-]	Saturated Hydraulic Conductivity [m/s]
Clay	1200	0.38	0.068	0.008	0.083	$5.60x10^{-7}$
Loam	1360	0.43	0.078	0.036	0.359	$2.89x10^{-6}$
Loamy Sand	1440	0.41	0.057	0.124	0.561	$4.05x10^{-5}$
Sand	1520	0.43	0.045	0.145	0.626	$8.25x10^{-5}$
Sandy Loam	1440	0.41	0.065	0.075	0.471	$2.89x10^{-6}$
Silt Loam	1280	0.45	0.067	0.020	0.291	$2.89x10^{-6}$
Weathered Bedrock	2100	0.08	0.01	0.067	0.308	$1.00x10^{-6}$
Bedrock	2500	0.01	0.005	0.004	0.636	$2.70x10^{-7}$

2.9 Simulation Specifications

The model was horizontally discretized into 50 by 50 m grid cells. The total simulation period, including spin up time, was from May 1st, 1982 to May 21st, 2023. The initial basic time step was 1 hour, while overland, unsaturated zone, and saturated zone flow had a maximum allowable time step of 24 hours. Results were stored as daily timesteps and hot starts were stored as monthly timesteps. Hot starts take the results of the previous simulation run to kick start (or hot start) the simulation, resulting in a faster initialization of the initial numerical solution. Results were computed using the final decade of the simulation period, from March 1st 2013 to May 21st 2023.

2.10 Model Calibration

The model was very difficult to run. Many attempts resulted in non-convergence, often due to dewatering of cells somewhere in the model domain.

The actual watershed boundary was expanded in the fan area (Figure 14) to attempt to better capture mountain front recharge. Ultimately, this led to numerical instabilities and non-convergence. Therefore, the model domain was reverted to the original watershed-defined domain for final calibration.

Because of a lack of continuous and long-term observational data, a conventional model calibration procedure was not carried out. Calibrating ungauged basins is particularly challenging and relies on best estimates of model input parameters and on subjective interpretation of the simulation results. In this study, model parameters were adjusted to best simulate snow accumulation and melt, and streamflow based on sparse nearby or near-in-time data. Therefore, this model is interpretative (scoping-level) in nature, and could be considered loosely calibrated. That is, this model is not uncalibrated, where steps were taken to adjust model parameters to best fit existing observational data.

Ensuring sufficient snowpack to generate the observed freshet peak, was particularly important for the stability of the entire model. We relied heavily on the Floe Lake Station SWE for snow accumulation timing rather than exact magnitude. We expect the seasonality of snow accumulation and melt at the Floe Lake Station to be similar to that in the WCW, although the magnitude is likely different due to site differences (elevation, slope aspect, vegetation, microclimate). Figure 17a compares observed SWE at the Floe Lake Station to simulated SWE in the WCW. Overall, modelled SWE timing was consistent with the observed data (correlation, r = .84), although magnitudes were clearly underrepresented, as expected.

The Windermere Creek hydrometric gauge was operational from 1959 to 1979, so these observed data were repeated (this allowed us to visualize observed data beyond the time of actual measurement). As a result, model calibration did not target exact flow magnitudes, but rather the general streamflow seasonality, which is relatively consistent over the years. Therefore, matching streamflow timing was a good indicator of model performance (Figure 17b). Streamflow in this region of B.C. is particularly dependent on the mountain snowpack, which was reflected in the model results. Simulated streamflow was consistently underestimated, especially during the baseflow recession period following the snowmelt peak in June. However, the overall pattern and timing was consistent with our expectations based on snowmelt (correlation, r = 0.53).

While VOW 10 is within 500 m of the watershed boundary, the well is located on the other side of a groundwater divide (see Figure 39 inset) and could not be used for calibration. Hydraulic conductivity values were found to have a large impact on numerical stability, often resulting in oscillations or model crashing if the values were too large. Similarly, ET parameters also impacted numerical stability, needing to be adjusted within the range of published literature values (Paudel, 2021). Model parameters subject

to adjustment, within a suitable range used in Voeckler et al. (2014) and Allen and Nott (2021), with their final values are shown in Table 5.

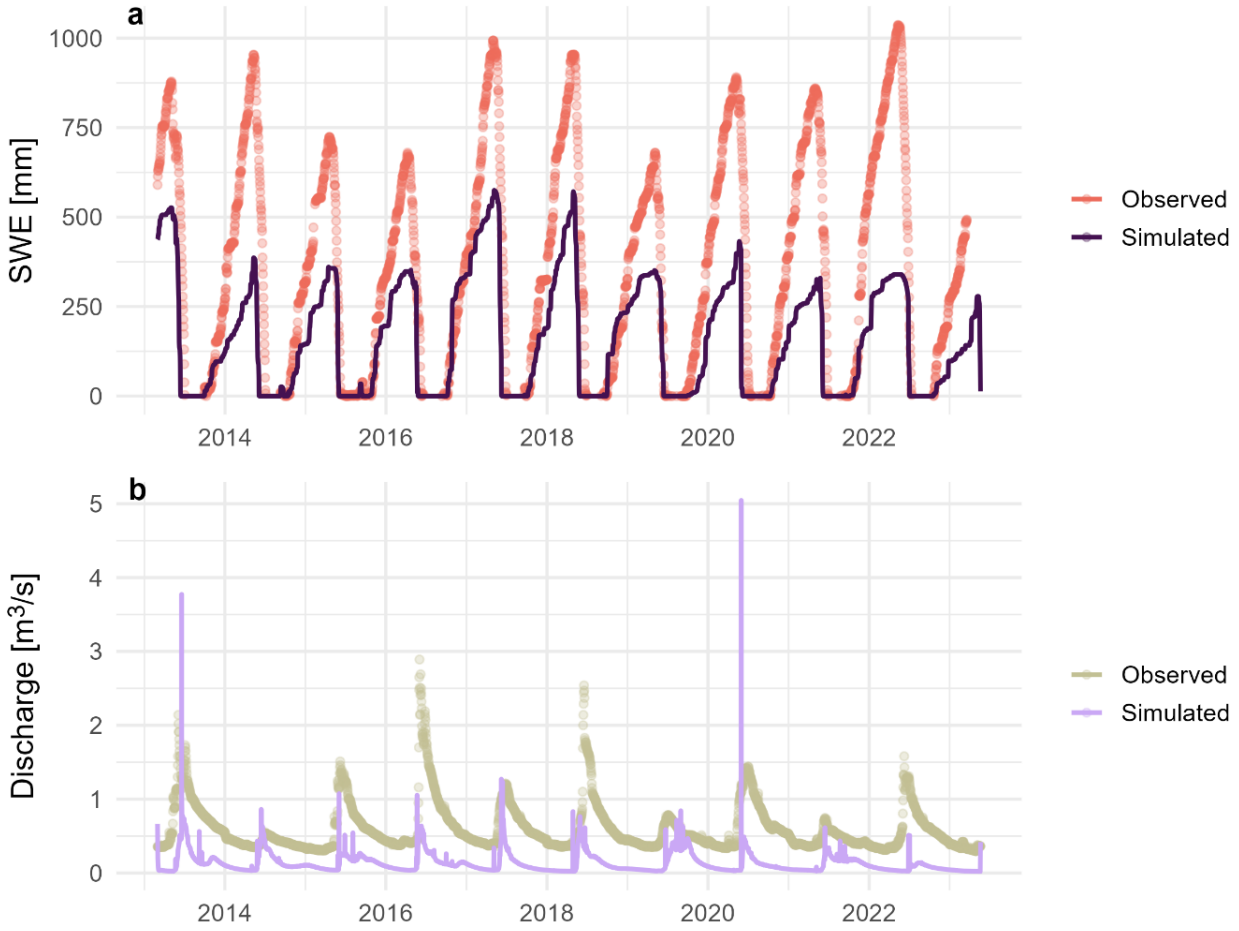

*Figure 17: (**a**) Simulated (WCW) and observed (Floe Lake Station) SWE and (**b**) simulated and observed (Windermere Creek Gauge) streamflow. Note that the Floe Lake Station is outside the catchment and the observed streamflow is not from 2013 to 2023, but simply a repetition of available historical data.*

Table 5: Final model parameters.

Module	Parameter		Initial	Calibrated
Climate	Precipitation Lapse Rate [%/100m]		10	15
	Temperature Lapse Rate [°C/100m]		-0.649	-1.1
	Temperature Wet Lapse Rate when Raining [°C/100m]		-0.3	-0.6
			0.5	0.3
	Degree Day Coefficient [mm/°C/day]		2	4
Land Use - Evapotranspiration	Canopy Interception [mm]		0.05	0.01
	C1 [-]		0.3	0.08
	C2 [-]		0.2	0.08
	C3 [mm/day]		20	2
	Aroot [m^{-1}]		0.25	0.1
MIKE HYDRO	Leakage Coefficient for Aquifer-River exchange [day^{-1}]		$1.0x10^{-8}$	$1.0x10^{-5}$
Saturated Zone	**Geological Lenses**	**Parameter**		
		Horizontal K [m/s]	**Vertical K [m/s]**	**Specific Yield [-]**
	Alluvial Fan (Unsaturated)	$1.7x10^{-6}$	$1.7x10^{-7}$	0.20
	Upper Aquifer (Saturated)	$5.8x10^{-6}$	$5.8x10^{-7}$	0.18
	Aquitard (Confining)	$1.0x10^{-8}$	$1.0x10^{-8}$	0.08
	Middle Aquifer (Confined)	$2.3x10^{-5}$	$2.3x10^{-6}$	0.10
	Lower Aquifer (Confined)	$2.3x10^{-5}$	$2.3x10^{-6}$	0.10
	Valley Fill (Alluvial Fan Material)	$1.7x10^{-6}$	$1.7x10^{-7}$	0.20

3. RESULTS

3.1 Precipitation and Snow Storage

Application of the precipitation lapse rate resulted in differential precipitation rates across the catchment depending on elevation (Figure 18). Resulting precipitation rates at the highest elevations in the WCW were up to three times the rate of precipitation at low elevation on any given day. More precipitation fell and was stored as snow at higher elevations (Figure 19).

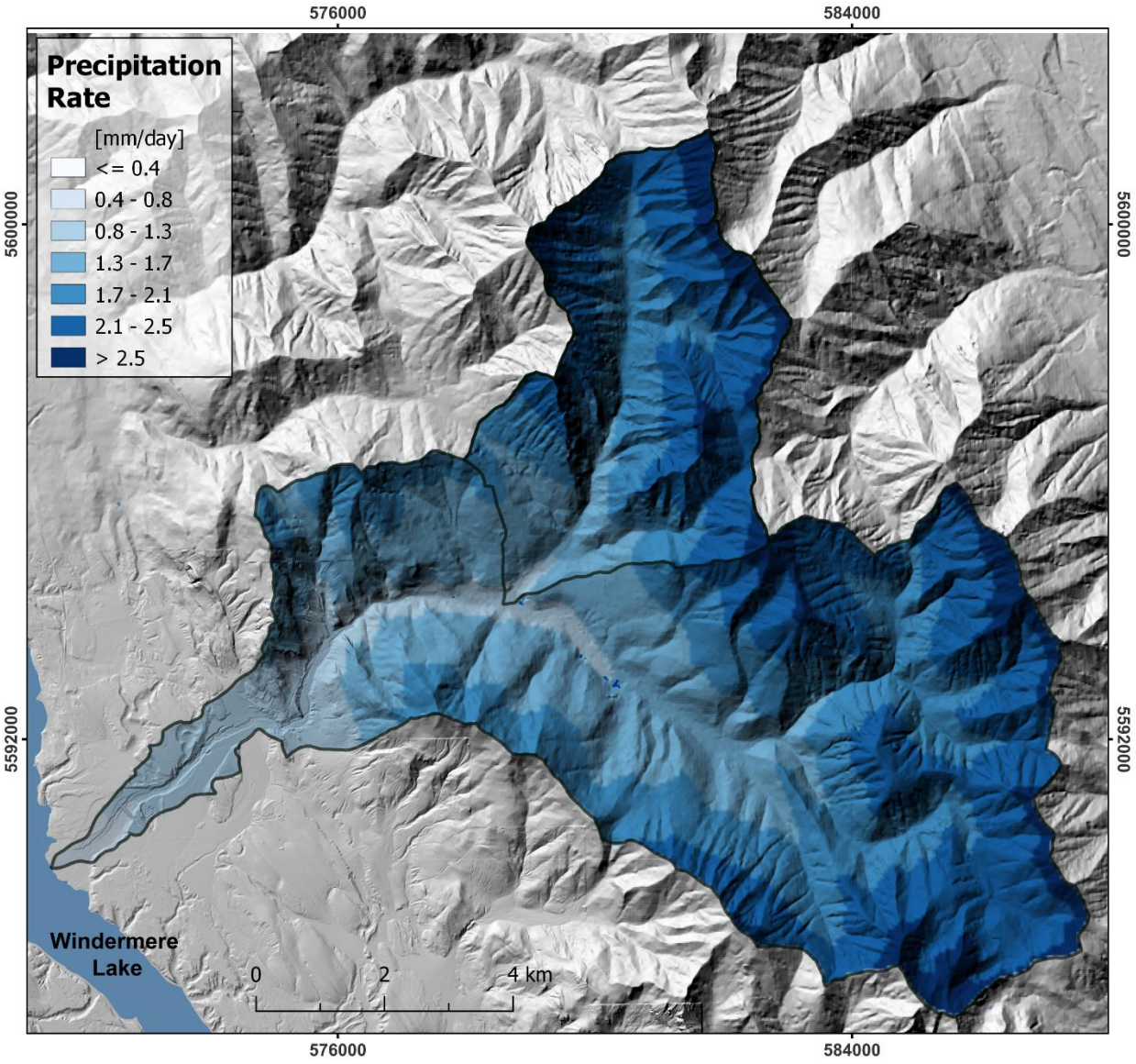

Figure 18. Average daily precipitation rate in the WCW.

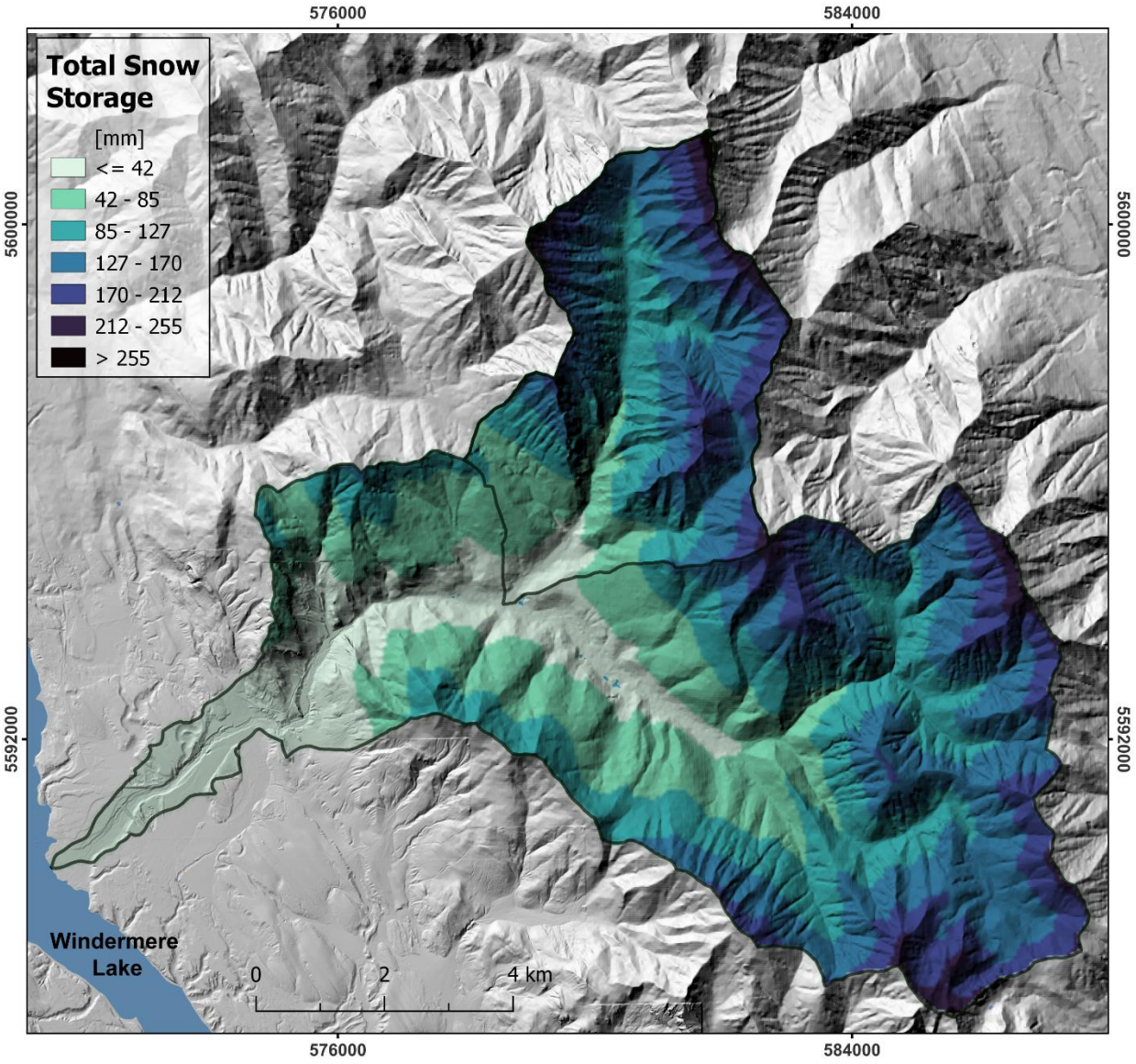

Figure 19. Average annual total snow storage in the WCW. Note this is snow depth, and not SWE.

3.2 Mean Groundwater Levels

The average annual hydraulic head or water table elevation map is shown in Figure 20. Greater hydraulic gradients were found in the mountainous areas of the catchment. This groundwater was efficiently drained to the valley bottoms and funnelled into the fan area, where the hydraulic gradient was much lower. There was a much greater component of downward vertical flow (map not shown) as groundwater entered the fan, where more accommodation space is present.

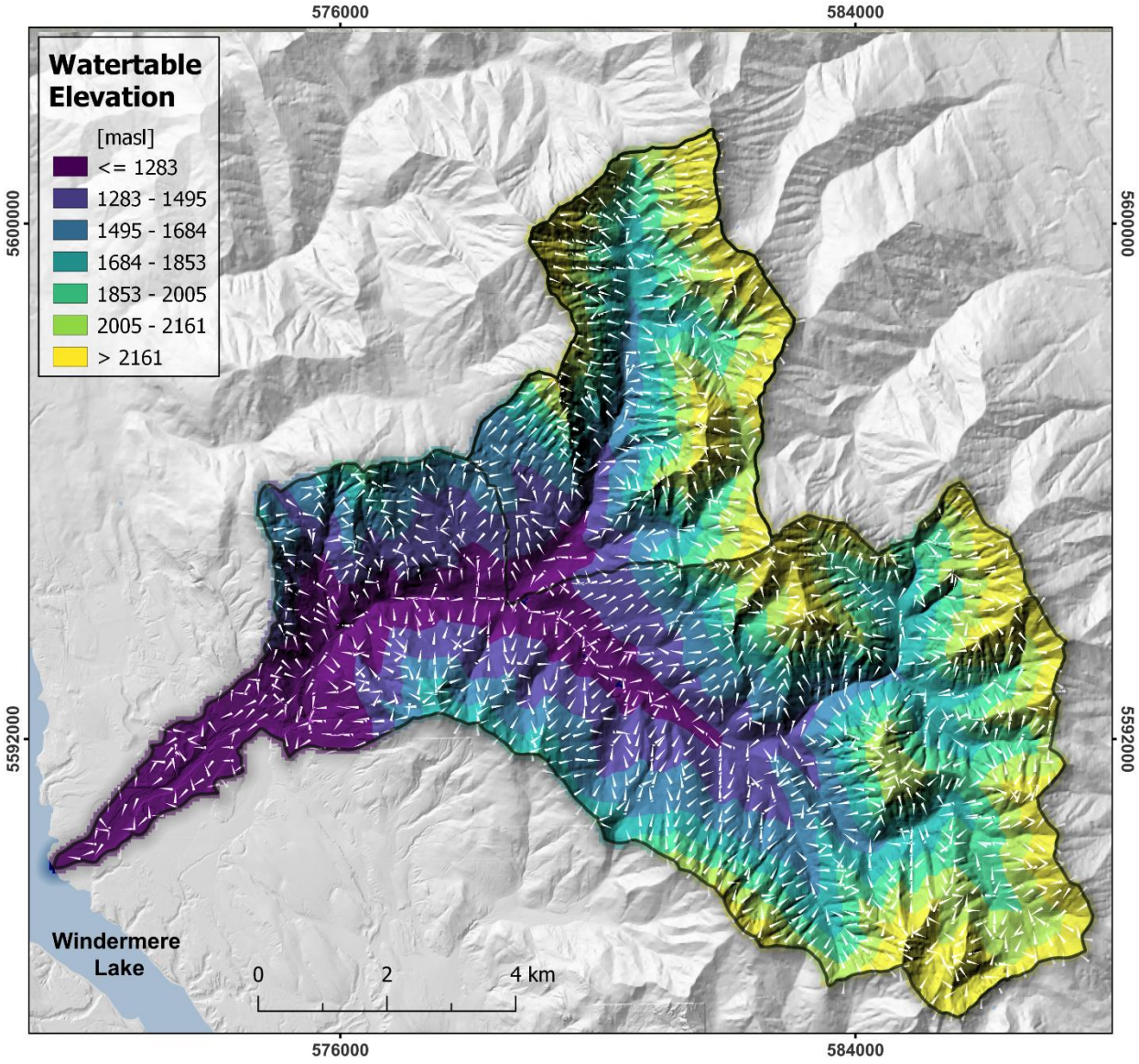

Figure 20: Average hydraulic head (water table elevation) in the saturated zone. Flow direction and magnitude vectors are shown by white arrows.

The depth to the water table is shown in Figure 21. The water table was generally at least 20 m deep along the mountain tops but was shallower on the slopes, reaching depths of at least 5 m. The water table could be at or above ground level in the mountain valleys as evidenced by lakes and wetlands in aerial imagery. Zooming into the alluvial fan zone of the catchment (Figure 22), the water table was generally within 5 m of the ground surface but could be up to 20 m deep in the higher topographic regions of the fan. A near or above surface water table within the deeply incised stream valley was consistent with observations from Natasha Neumann (October 2022 field survey), noting several wetland areas (see Figure 38) and springs at the fan apex (Figure 22).

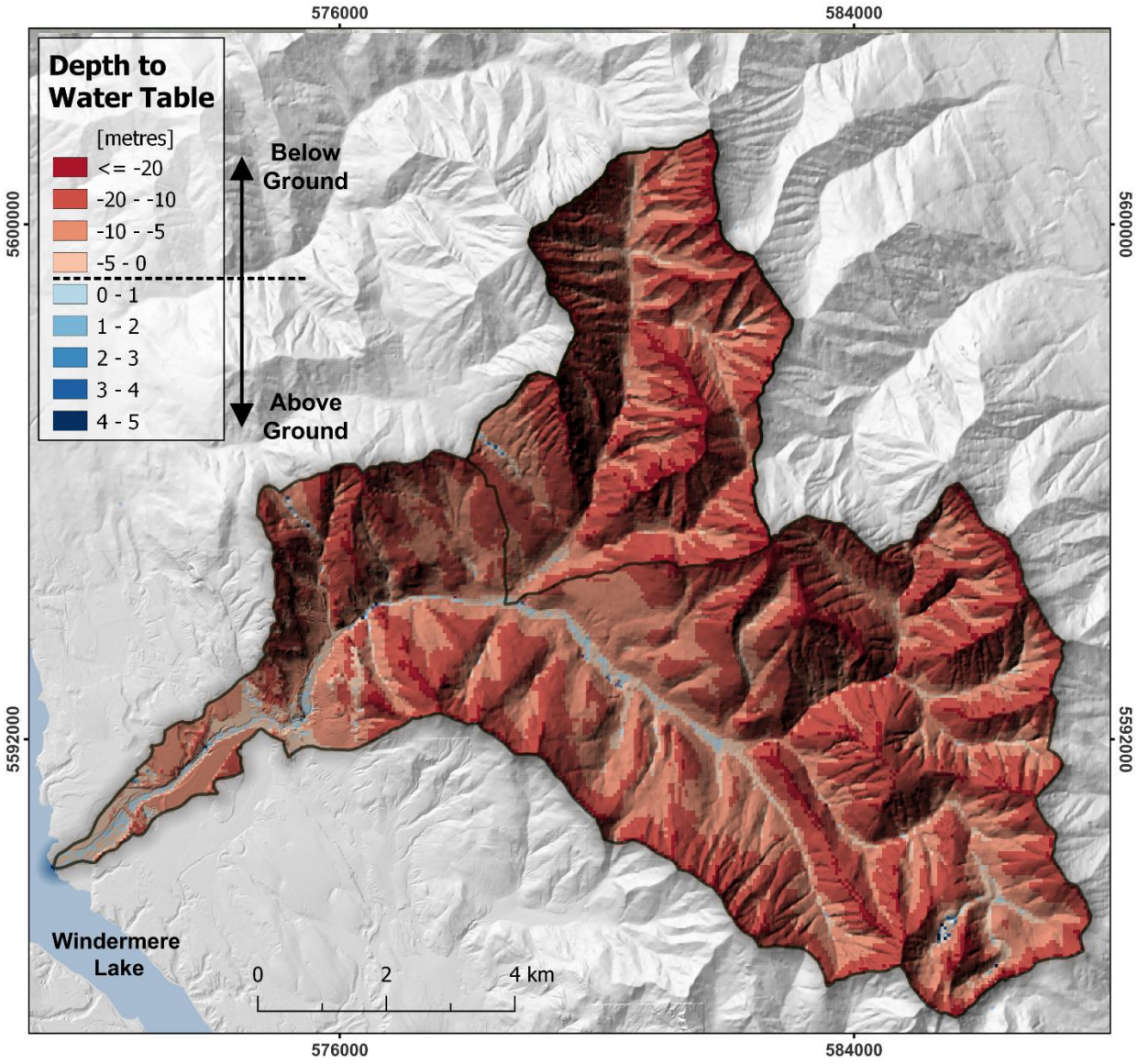

Figure 21: Average depth to water table in the WCW.

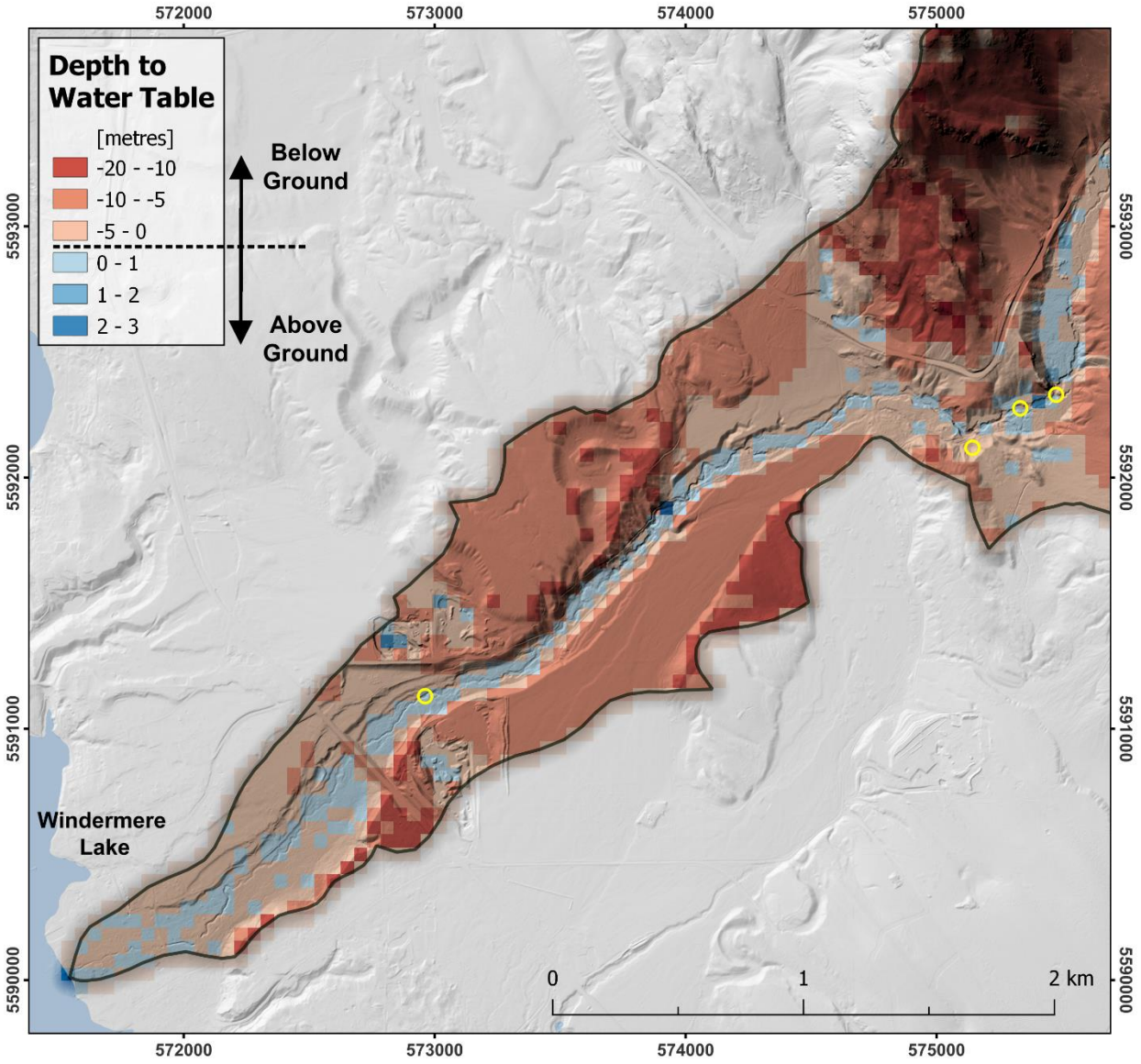

Figure 22: Average depth to water table in the fan area. Known groundwater spring locations are shown by yellow circles.

3.3 Recharge and Discharge

Recharge occurs when there is a transfer of water from the unsaturated zone (UZ) to the saturated zone (SZ); that is, the flow of groundwater is downward. Discharge is the opposite, that is, flow is upward from the SZ to the UZ. MIKE SHE calculates recharge values anywhere and any time there is a downward transfer of water so if groundwater recharges at high elevation, and then discharges at some point further down gradient, flows overland for some distance and recharges again, then MIKE SHE accounts for both recharge events in the water balance. This means that MIKE SHE overestimates recharge, and consequently, it is best to think of recharge and discharge as simply transfers to and from the UZ and SZ. That said, maps of recharge and discharge (or seepage) and graphs showing the timing and location of recharge are very useful.

Average monthly recharge, or transfers to, the saturated zone are shown in Figure 23. The largest recharge rates were calculated where the largest precipitation and SWE occurred, in the high mountain ranges. Discharge occurred to lakes and streams in mountain ravines and valleys.

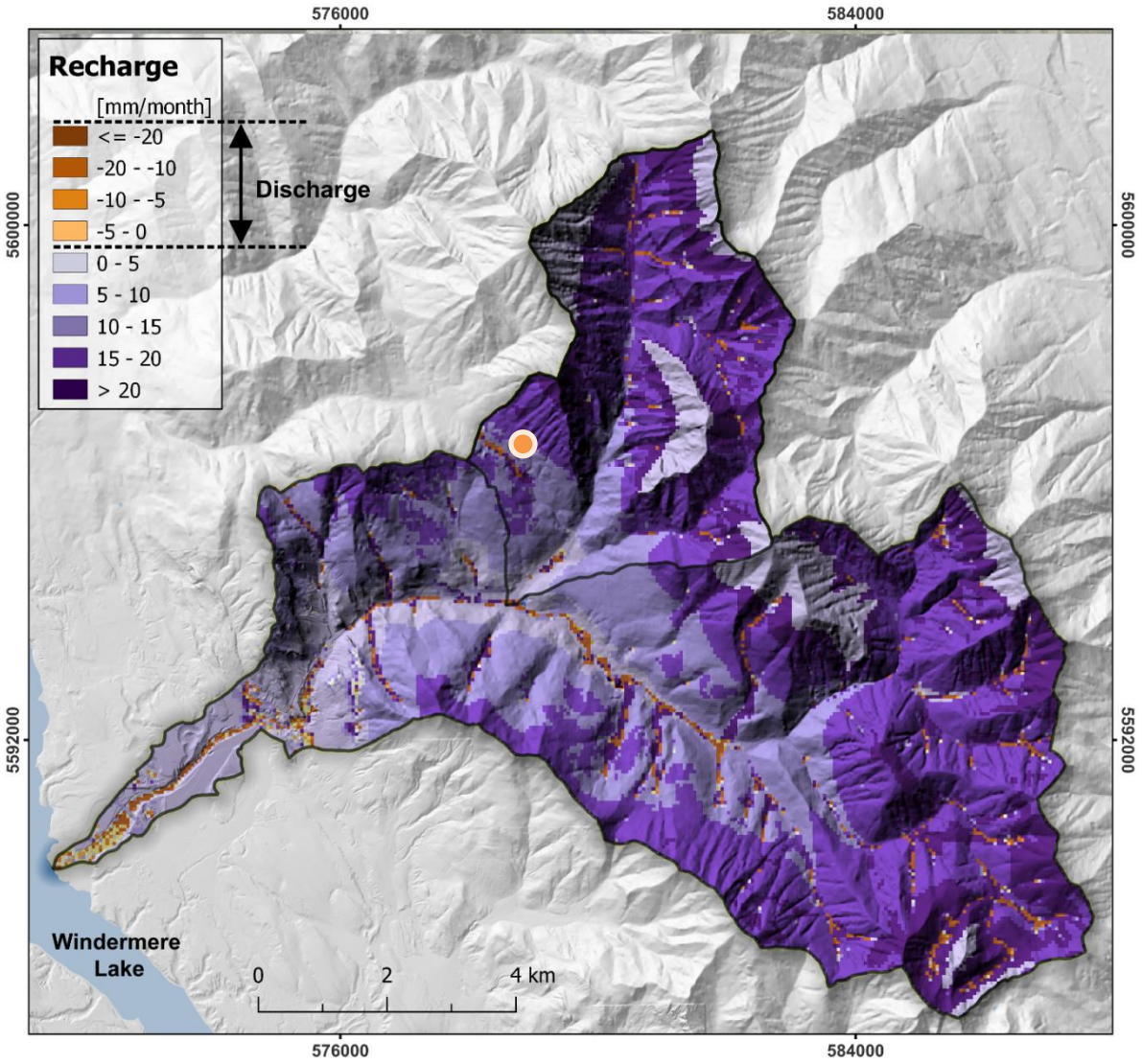

Figure 23: Average monthly recharge to saturated zone. Note that values represent transfers between the UZ and SZ. The orange dot represents a point where a time series was extracted, shown in Figure 26b.

Zooming in to the fan area (Figure 24), recharge values were much smaller than in the mountainous portions of the catchment. There was a highly localized recharge area at the mountain front where the sediment thickness increases. Much of the groundwater discharged into the stream valley, contributing baseflow to wetlands and streams. Groundwater springs, as previously confirmed by Natasha Neumann (Oct. 2022 field survey), were common within the stream valley.

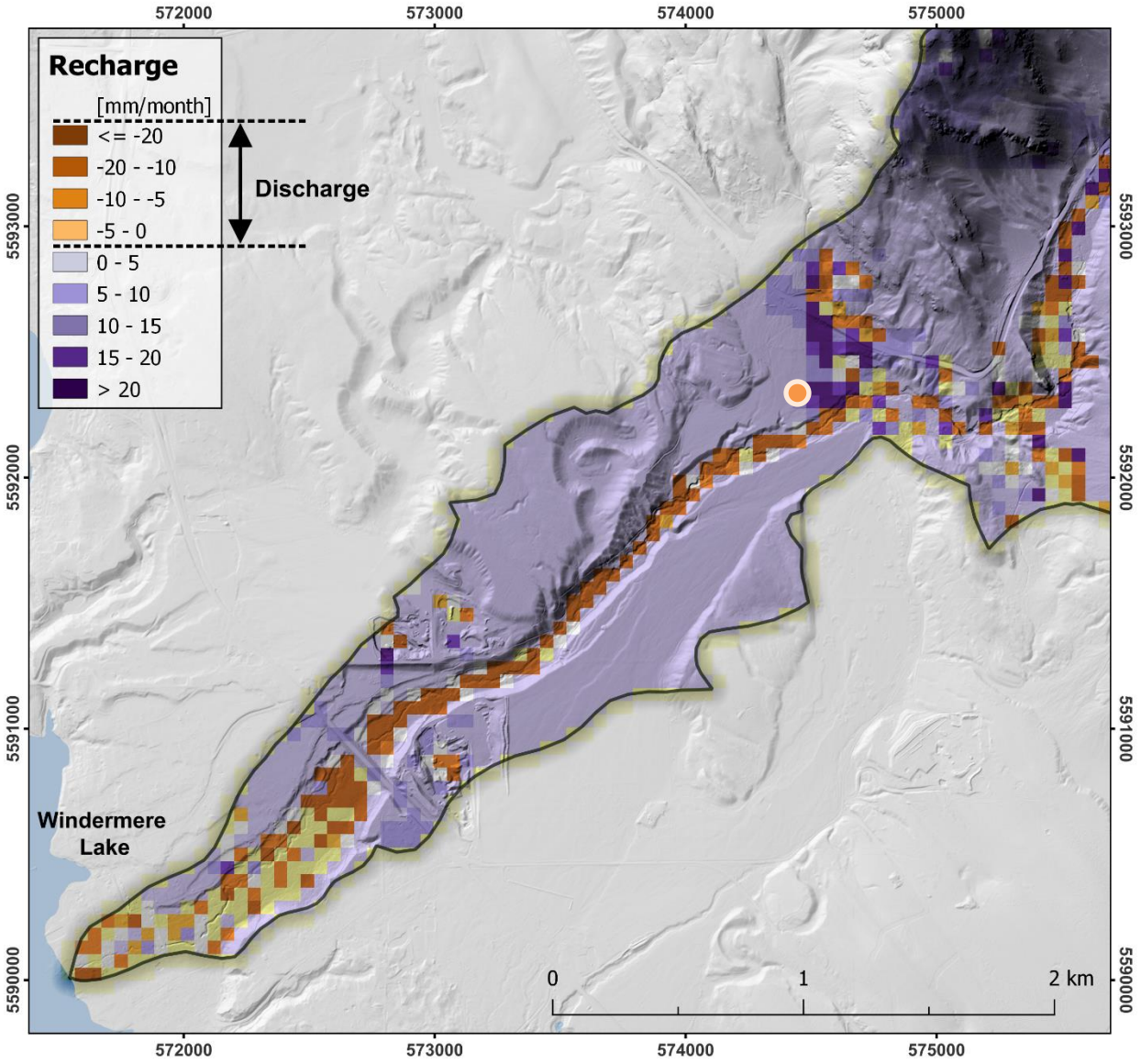

Figure 24: Average monthly recharge to the saturated zone in the fan area. The orange dot represents a point where a time series was extracted, shown in Figure 26a.

Figure 25a shows the simulated depth to the water table and recharge at a point in the fan apex (see Figure 24 for location) and at a point in the mountains (see Figure 23 for location). Comparing patterns of recharge and groundwater level, it would seem that at least near the fan apex, groundwater levels tended to peak in late autumn to early winter (Figure 25a). This was not entirely unexpected because in the fan area snowpack accumulation would begin later, as temperatures are warmer and precipitation falling on the fan would likely fall as rain (Figure 4). In contrast, the snowpack in the mountain block begins to accumulate in the late fall around early November (Figure 25b). Groundwater levels in the mountain block tended to consistently peak around the end of June, coinciding with peak snowmelt.

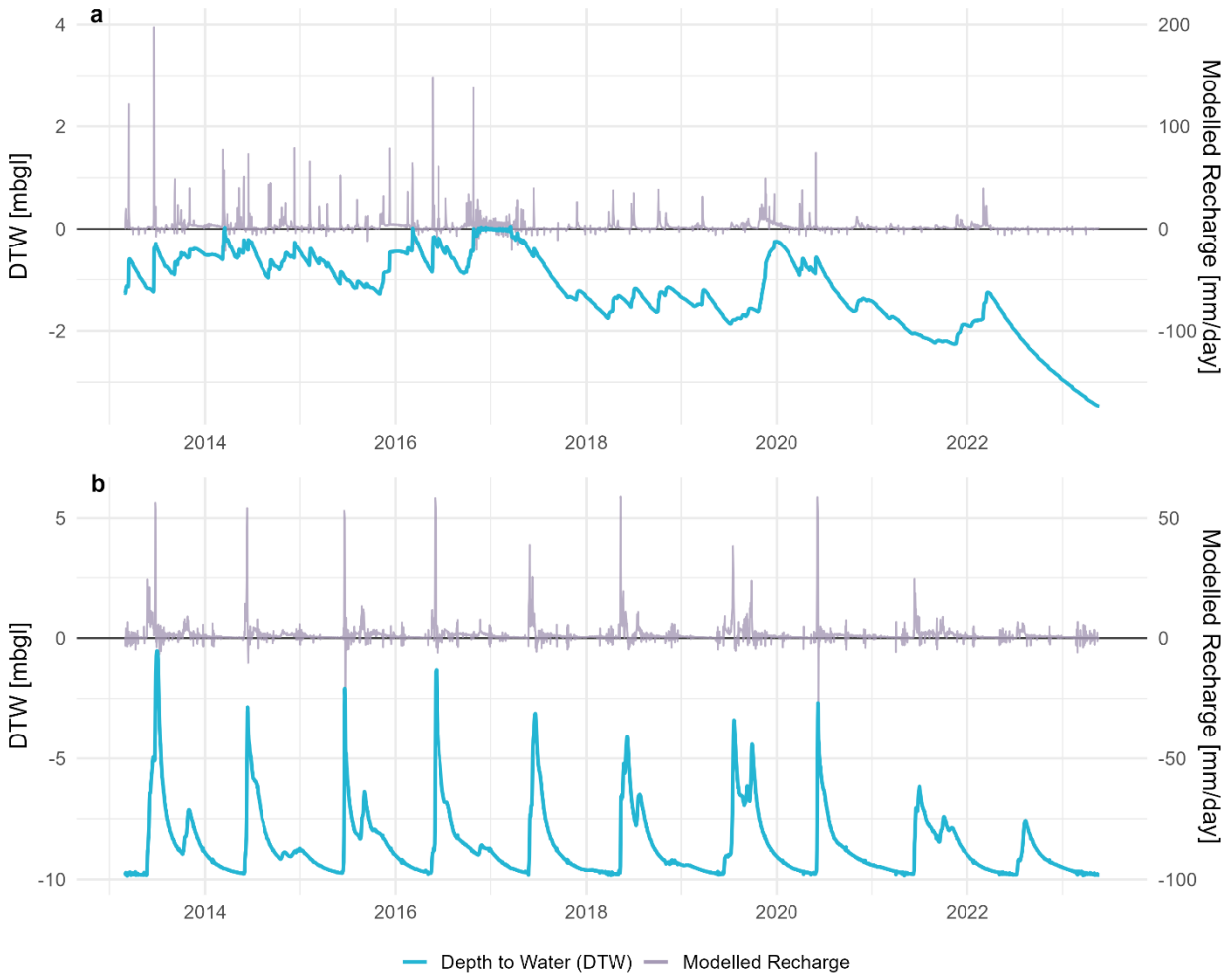

Figure 25: (a) Simulated depth to the water table and recharge at a point in the fan apex, shown in Figure 24. Depth to water (DTW) is represented as metres below ground level (mbgl). (b) Simulated depth to the water table and recharge at a point in the mountainous portion of the WCW, shown in Figure 23.

At the catchment scale, monthly average simulated recharge (i.e., the transfer of water from the UZ to the SZ) is shown in Figure 26a. Recharge was highest during the June and July snowmelt pulse. The least amount of recharge occurred in April and May when the snowpack was at its peak and rainfall was low. As noted above, the recharge values were overestimated due to how MIKE SHE computes recharge.

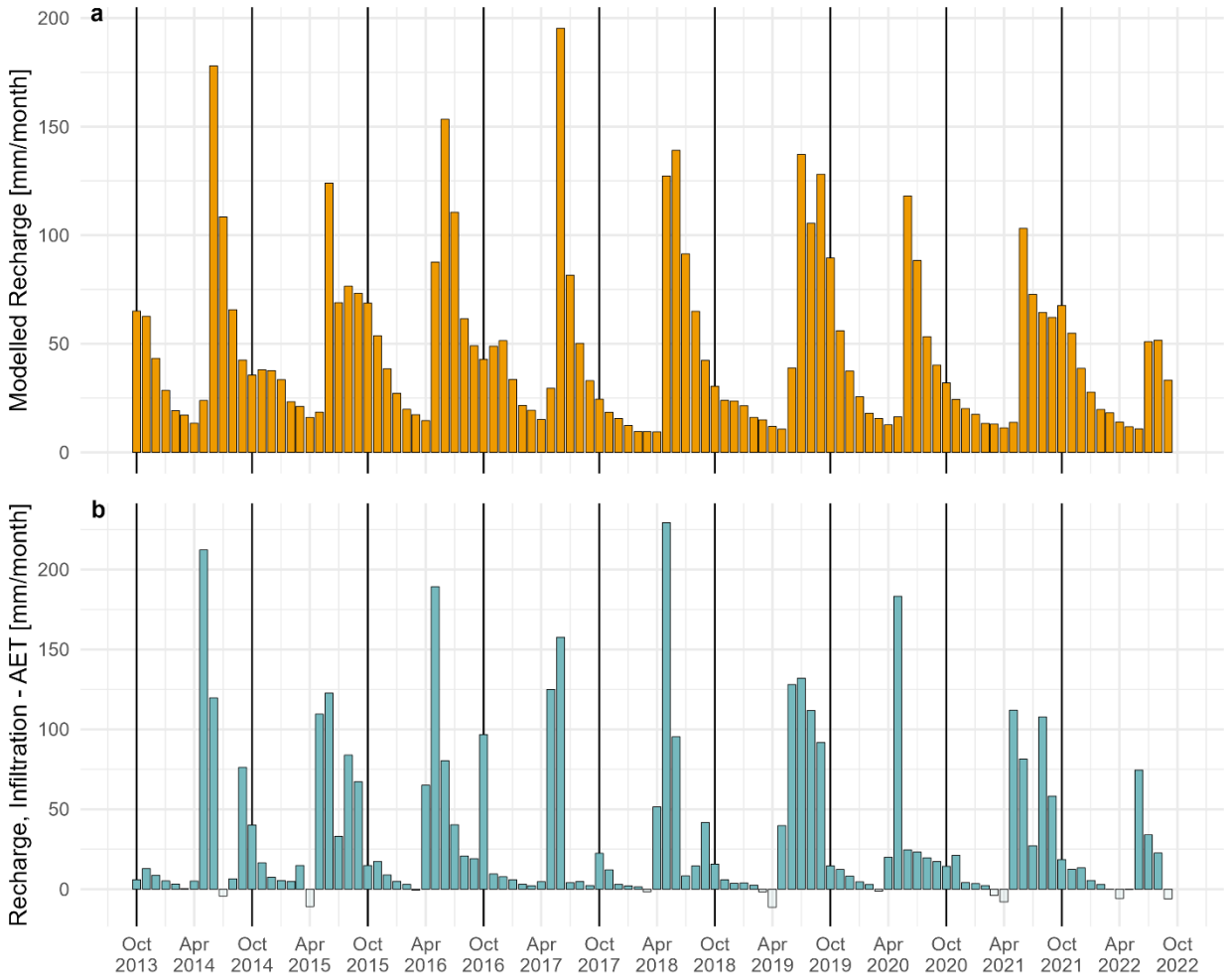

Figure 26. (a) Catchment averaged monthly simulated "recharge" (transfers to SZ). (b) Recharge as computed using a mass balance approach by subtracting actual evapotranspiration from infiltration. Black lines separate water years.

Because MIKE SHE misrepresents the recharge amount, as an alternative for estimating recharge, we used a simple mass balance approach based on individual simulated outputs: subtracting actual evapotranspiration (AET) from infiltration (I). Infiltration includes all precipitation (P) water that makes it to the vadose zone that was not intercepted via overland (OL) flow (or canopy storage) or converted to snow via snow storage change (SSC). Recharge as represented using this mass balance approach showed recharge as more discrete in time (Figure 26b) rather than as a continuous input as modelled (Figure 26a). This intuitively makes sense, as there would be essentially no recharge during cold periods as the snowpack is accumulating.

3.4 Annual Water Balances

The yearly aggregated water balance results (per water year – October 1 to September 30) are shown in Table 6 and Figure 27. On average, just under 700 mm of precipitation (elevation corrected) was received by the catchment. This precipitation was partitioned to different components of the water balance. Approximately 31% of precipitation was returned to the atmosphere via evapotranspiration

and about 20% of precipitation contributed to streamflow via overland flow. While the average AET of 218 mm seemed low, it was consistent with the 1 km resolution average annual evapotranspiration product from MODIS satellite data (ESRI HYDRO, 2020). This interactive map showed an average annual (2000 to 2011) AET of 263 mm over a small sub-basin of the Upper Columbia River Basin (including the WCW). 91% of precipitation that falls as rain or is melted from the snow pack gets infiltrated into the vadose zone. Using a simple mass balance approach, described above, by subtracting actual evapotranspiration (AET) from infiltration (I), 60% (91% Infiltration - 31% AET) of precipitation goes to recharge (R) (Table 6). This was a more realistic number compared to the simulated transfers to the SZ via the UZ, which over-estimated recharge as 82% of precipitation (Table 6). Groundwater recharge seemed to be more sensitive to precipitation than evapotranspiration. Comparing the 2015 water year to the 2017 water year, AET values were similar but there was an 85 mm difference in precipitation, which resulted in a recharge difference of over 71 mm.

Change in subsurface (SZ and UZ) storage was quite variable from year to year, averaging at -20 mm (Table 6) and indicating long-term withdrawal from subsurface water storage. During water years with near or above normal precipitation and negative storage change, this additional water released from storage tended to inflate the SZ to river amounts. The SZ to river component represents baseflow contributions to streamflow via groundwater discharge. A significant amount of groundwater contributed to streamflow. This was consistent with both the relatively long baseflow recession in Figure 7 and the fact that, at least in the mountain block, the main direction of groundwater discharge was toward the stream valleys.

Table 6: Annual water balance components (mm/year) for individual water years over the last decade of the simulation period (2013 to 2023). (P) Precipitation, (I) Infiltration, (AET) Actual Evapotranspiration, (OL) Overland flow, (SZ) Saturated Zone, (UZ) Unsaturated Zone. Transfer to SZ is reported in the unsaturated zone water balance as recharge but overestimates the actual recharge amount. An alternative (and more realistic) recharge estimate is made by subtracting AET from I.

Water Year	**Water Balance Components**						**Unsaturated Zone Water Balance**		**Calculated Recharge**
	P	**I**	**AET**	**OL to River**	**SZ to River**	**Snow Storage Change**	**Transfer to SZ**	**SZ & UZ Storage Change**	**I – AET**
2013-14	703	670	219	154	417	-7.5	667	-81	451
2014-15	774	717	222	134	353	0.1	566	63	494
2015-16	767	712	249	167	438	0.2	702	-88	463
2016-17	689	637	214	157	390	-0.2	622	-73	423
2017-18	763	699	219	132	350	2.0	564	60	480
2018-19	831	746	224	141	334	-0.5	563	136	521
2019-20	622	536	207	194	382	-1.4	571	-161	329
2020-21	714	646	226	91	286	0.0	448	110	420
2021-22	391	350	179	86	272	0.2	399	-148	171
Average **(% of P)**	695	635 (**91%**)	218 (**31%**)	139 (**20%**)	358	-1	567 (**82%**)	-20	417 (**60%**)

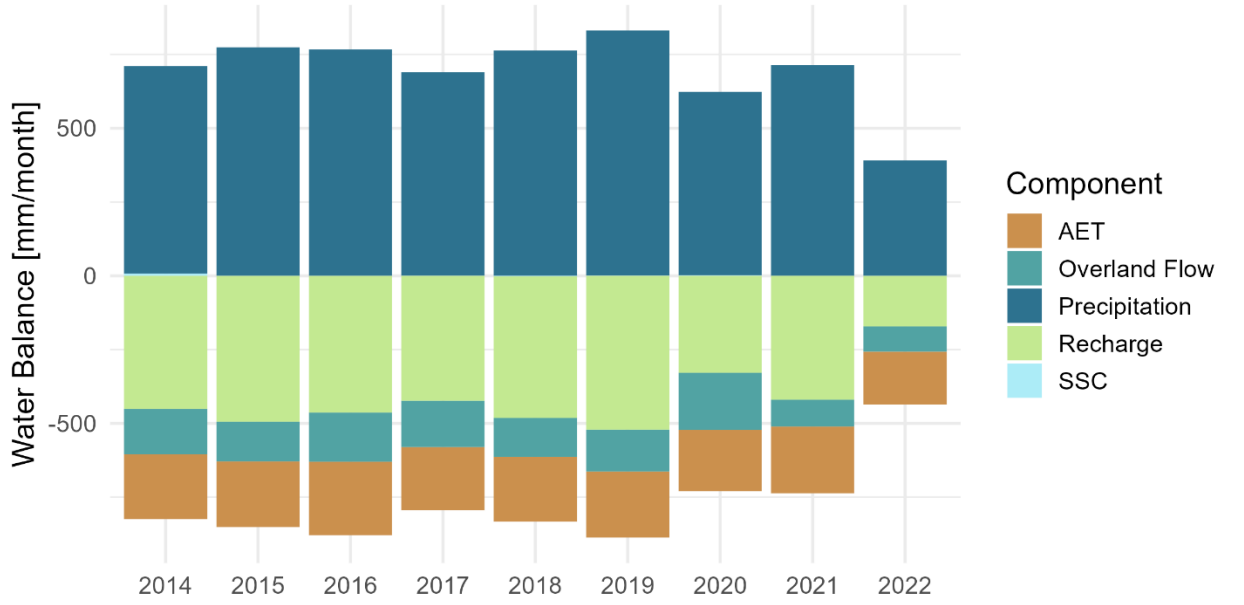

Figure 27. Water year water balance components.

3.5 Mean Monthly Water Balance

Average seasonal patterns for transfers of water within the catchment is shown in Table 7. Precipitation was relatively constant through the year but tended to peak from May to July. Accordingly, AET increased during this period, coincident with higher temperatures. Additionally, infiltration also peaks as the higher temperatures melt the snowpack, where infiltration surpasses precipitation. AET was low from October to March, when the weather was colder, and the snowpack was accumulating. AET was a difficult parameter to calibrate, and while the model results suggest zero AET in December and January, this was likely an underestimate.

Focusing on the pattern rather than the magnitude of transfer of water to the SZ, the majority of recharge occurred from May to September, from both rainfall and snowmelt. Focusing on subsurface storage changes, April, May, and June showed the only positive changes (i.e., inflows to the UZ and SZ) while transfers to the SZ peaked in June and July. This would suggest that rapid snowmelt (highly negative snow storage changes) immediately enters the unsaturated zone as a large pulse but takes about one additional month to the reach the SZ. Snowmelt generally begins in April, once snow storage becomes negative, while snow begins to accumulate by October.

Again, considering a simple mass balance approach by subtracting AET from I results in a very different pattern and magnitude of available recharge (Table 7). The effects of SSC on infiltration are much clearer on a month-by-month basis than annually.

Take February, for example, where nearly all precipitation falls as snow, stored in the snowpack and unavailable for recharge. Infiltration, AET, and OL flow are quite low (I and OL likely resulting only from seepage) during this time, thus we would expect little to no recharge in February. Low recharge months are associated with negative changes in subsurface storage. As temperatures began to increase starting in April, precipitation begins to fall as rain, and the snowpack begins to melt. May to September represents the major recharge months which is comparable to using the patterns of transfers to SZ, but with a much more accurate magnitude. Looking at the month of May, the majority of snowpack melt has

taken place and all precipitation falls as rain (or as snow that melted quickly), resulting in a recharge pulse (Figure 28) closely matching the hydrograph rise and pulse of Windermere Creek (Figure 7).

Table 7: Monthly average water balance components (mm/month) over the last decade of the simulation period (2013 to 2023). (P) Precipitation, (I) Infiltration, (AET) Actual Evapotranspiration, (OL) Overland flow, (SZ) Saturated Zone, (UZ) Unsaturated Zone. Transfer to SZ is reported in MIKE SHE as recharge but overestimates the actual recharge amount. An alternative (and more realistic) recharge estimate is made by subtracting AET from I.

Month	**Water Balance**						**Unsaturated Zone Water Balance**		**Calculated Recharge**
	P	**I**	**AET**	**OL to River**	**SZ to River**	**Snow Storage Change**	**Transfer to SZ**	**SZ & UZ Storage Change**	**I - AET**
January	63	4	0	6	19	63	25	-25	4
February	30	3	1	4	14	29	18	-18	3
March	36	8	7	4	12	27	16	-15	1
April	37	38	26	4	10	-19	13	17	12
May	92	190	56	15	16	-154	38	158	133
June	92	144	46	27	59	-73	118	31	98
July	59	69	36	22	57	-8	90	-47	33
August	65	68	25	16	45	0	66	-20	44
September	55	57	16	14	38	0	56	-12	41
October	71	32	5	12	35	46	51	-26	27
November	64	13	0	9	29	58	42	-32	13
December	32	7	0	8	25	31	34	-31	7
Sum **(% of P)**	695	635 (**91%**)	218 (**31%**)	139 (**20%**)	358	-1	567 (**82%**)	-20	417 (**60%**)

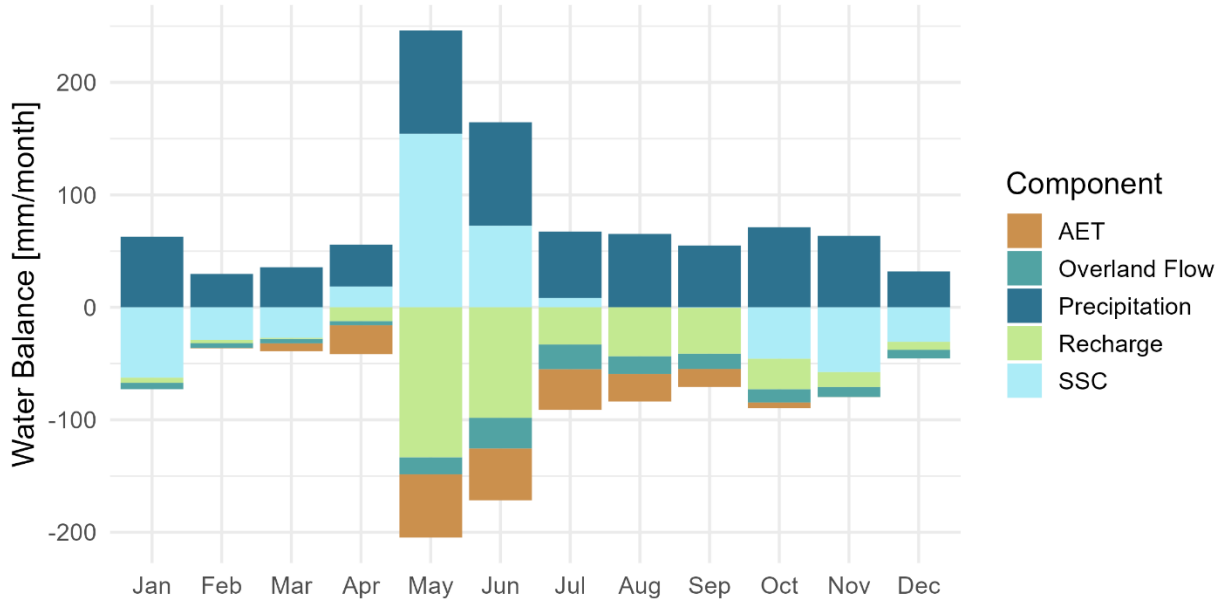

Figure 28. Average monthly water balance components.

3.6 GW-SW Interactions

SZ to river exchange represents the baseflow contribution of the groundwater system to the stream system. These groundwater-surface water (GW-SW) interactions are shown in Figure 29. Most notably, losing conditions were modeled in very few stream sections. That is, groundwater was almost always contributing to baseflow within the catchment. There were probably localized zones that did contribute to groundwater recharge but, at the scale used in this project (50 m cell size), the general pattern was that of gaining conditions nearly all the time. Back and forth exchanges between the stream and aquifers may occur at a much smaller scale than what is being represented in this model.

Most high volumetric exchanges tended to occur within the mountainous region where there was less subsurface storage. In contrast, in the fan the exchange volumes were lower, as there was more subsurface storage available for groundwater to occupy and less overall contribution to baseflow. The model cells also seemed to be disconnected in some areas, indicating that no exchange took place between the SZ and stream. Figures 30, 31, 32, and 33, show the seasonal means as represented by the months of January, April, July, and October, respectively.

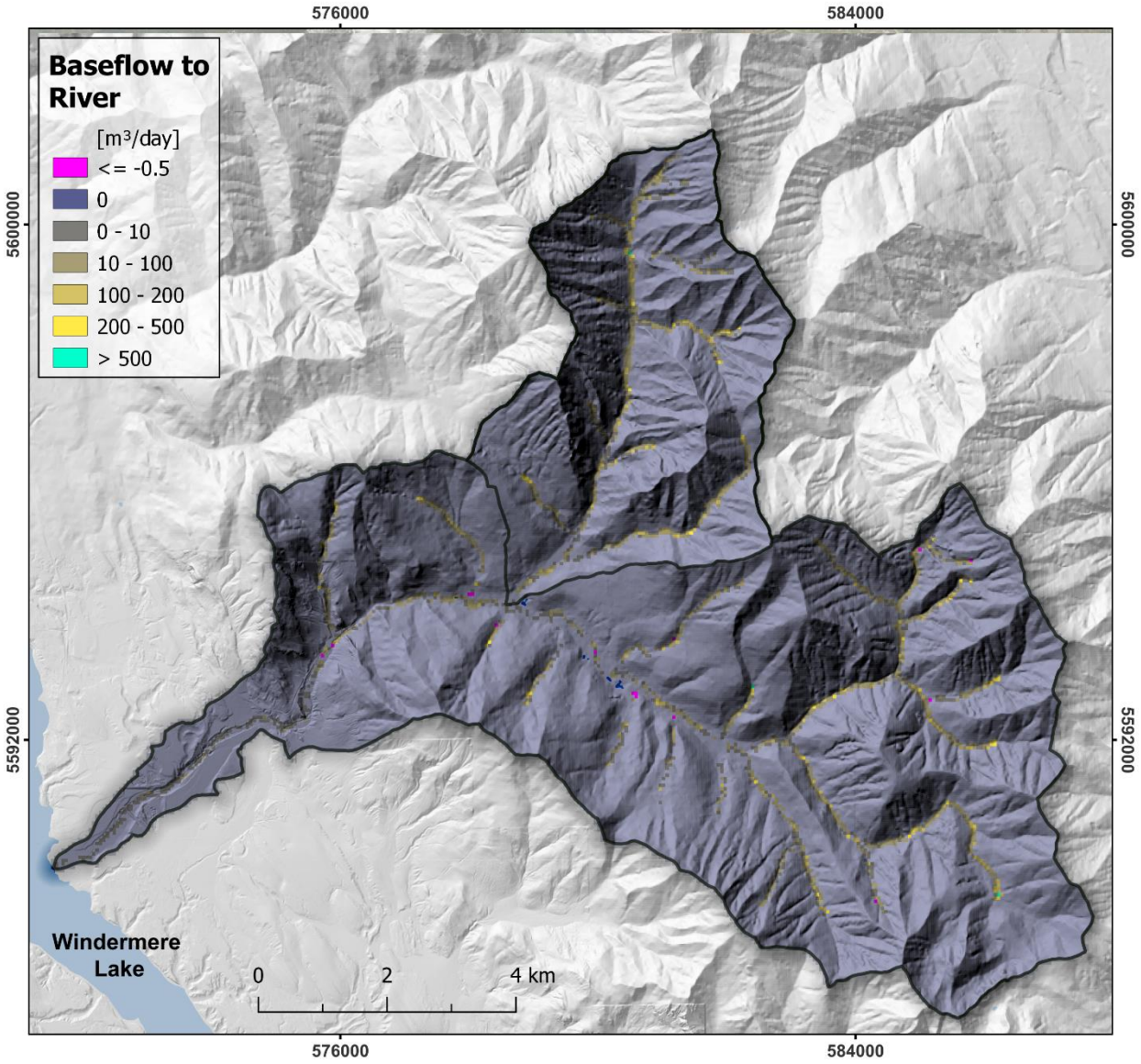

Figure 29: Annual average baseflow contributions from groundwater to Windermere Creek.

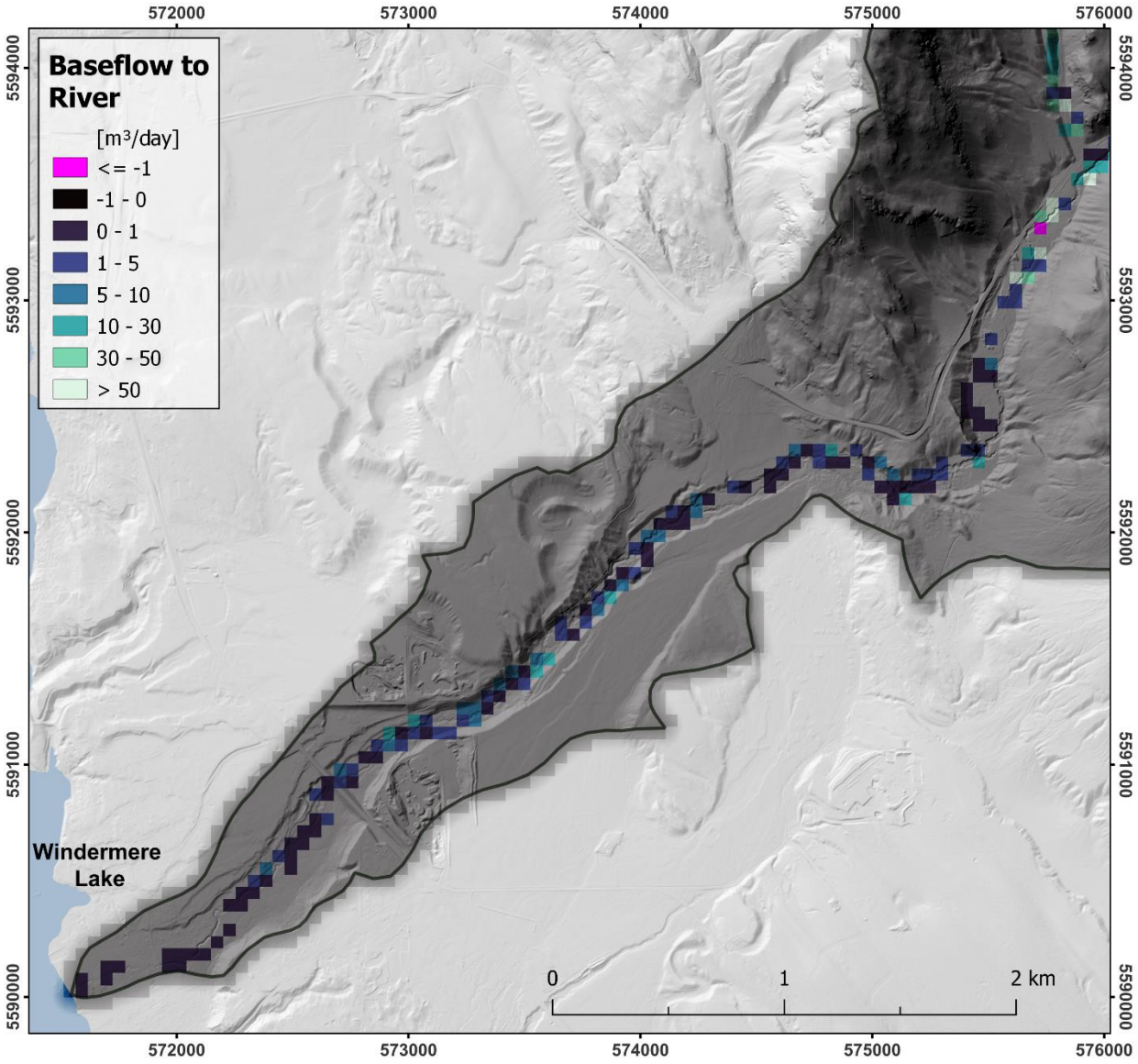

Figure 30: Average January baseflow contributions from groundwater to Windermere Creek in the fan area.

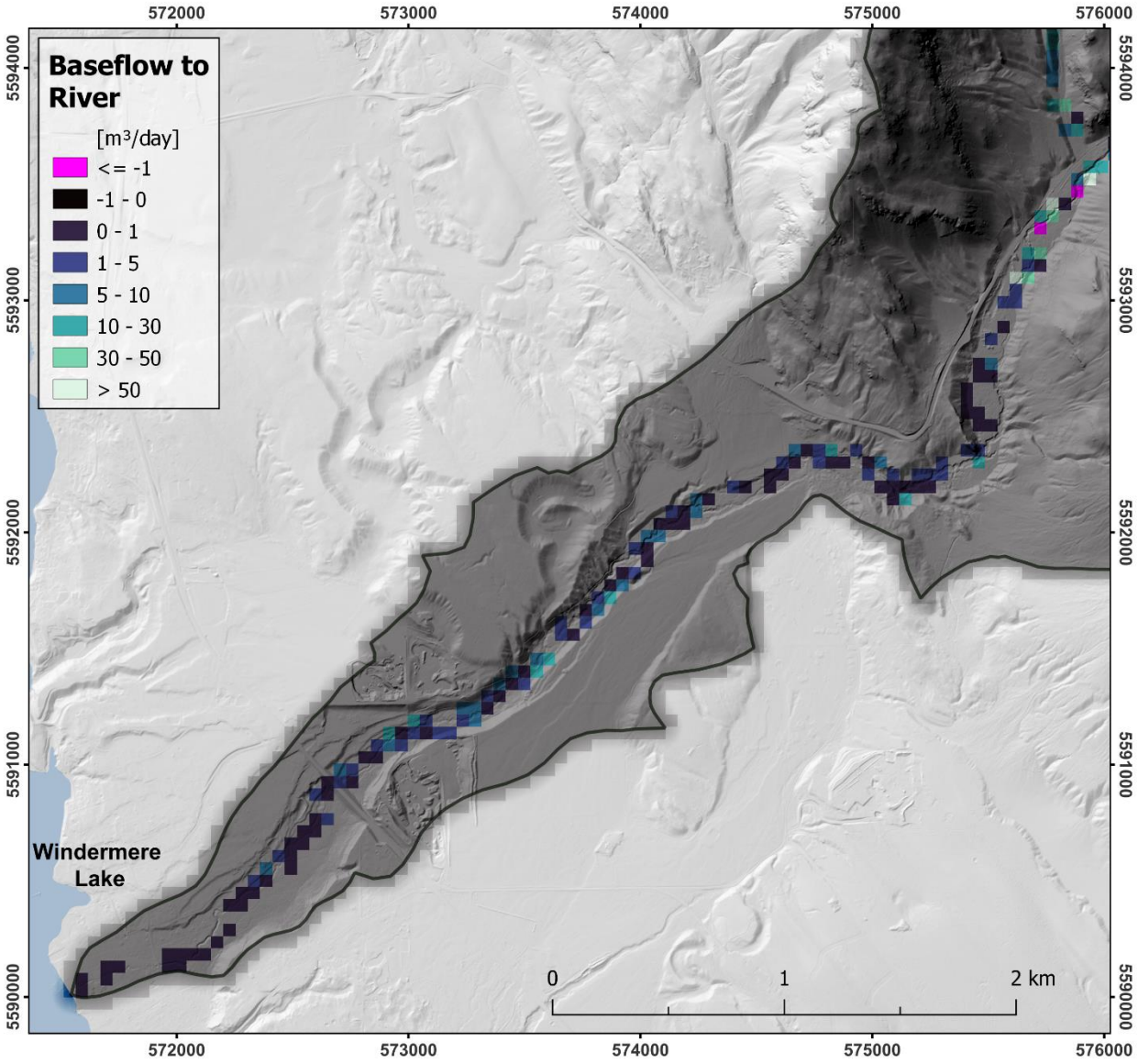

Figure 31. Average April baseflow contributions from groundwater to Windermere Creek in the fan area.

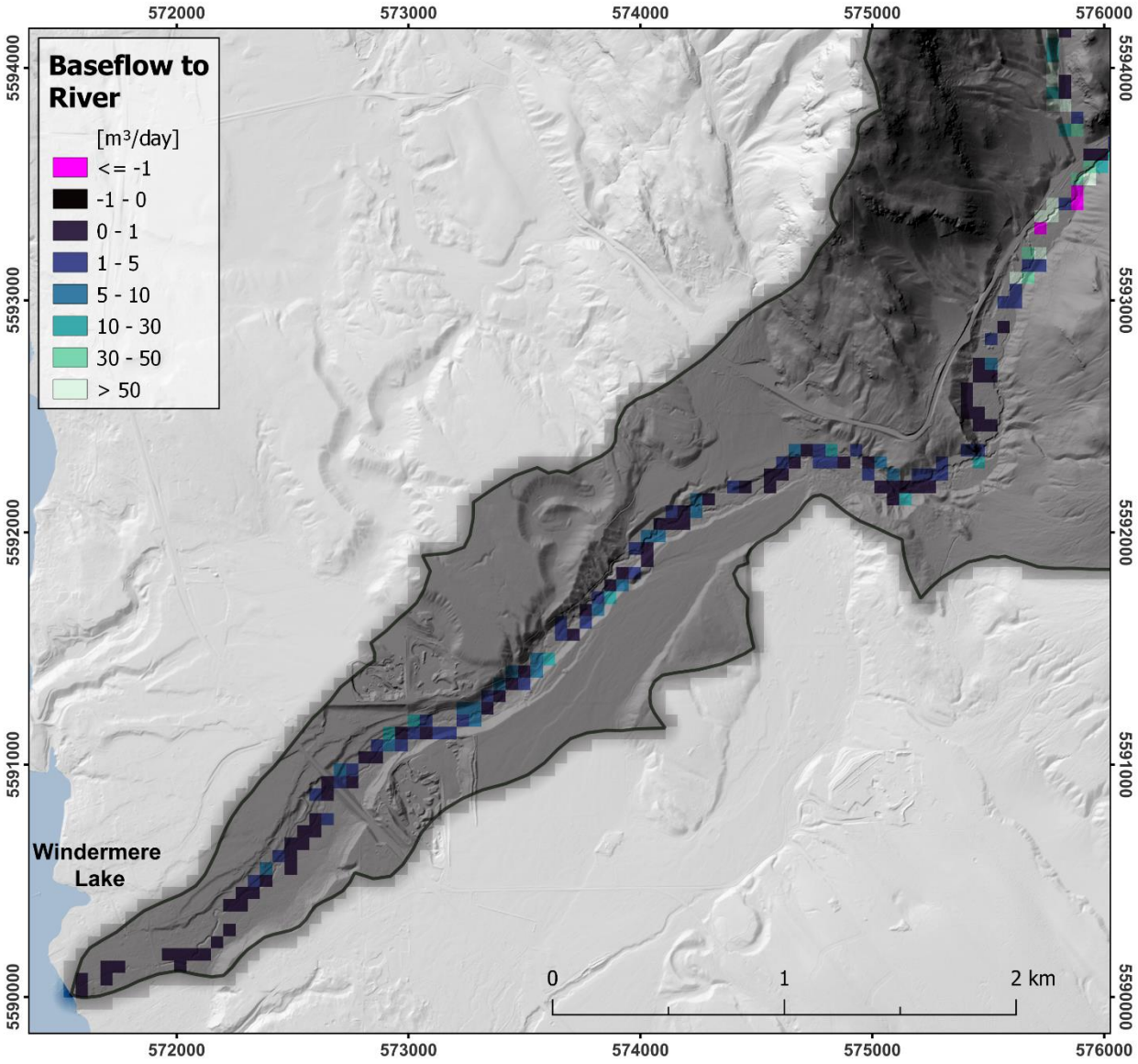

Figure 32. Average July baseflow contributions from groundwater to Windermere Creek in the fan area.

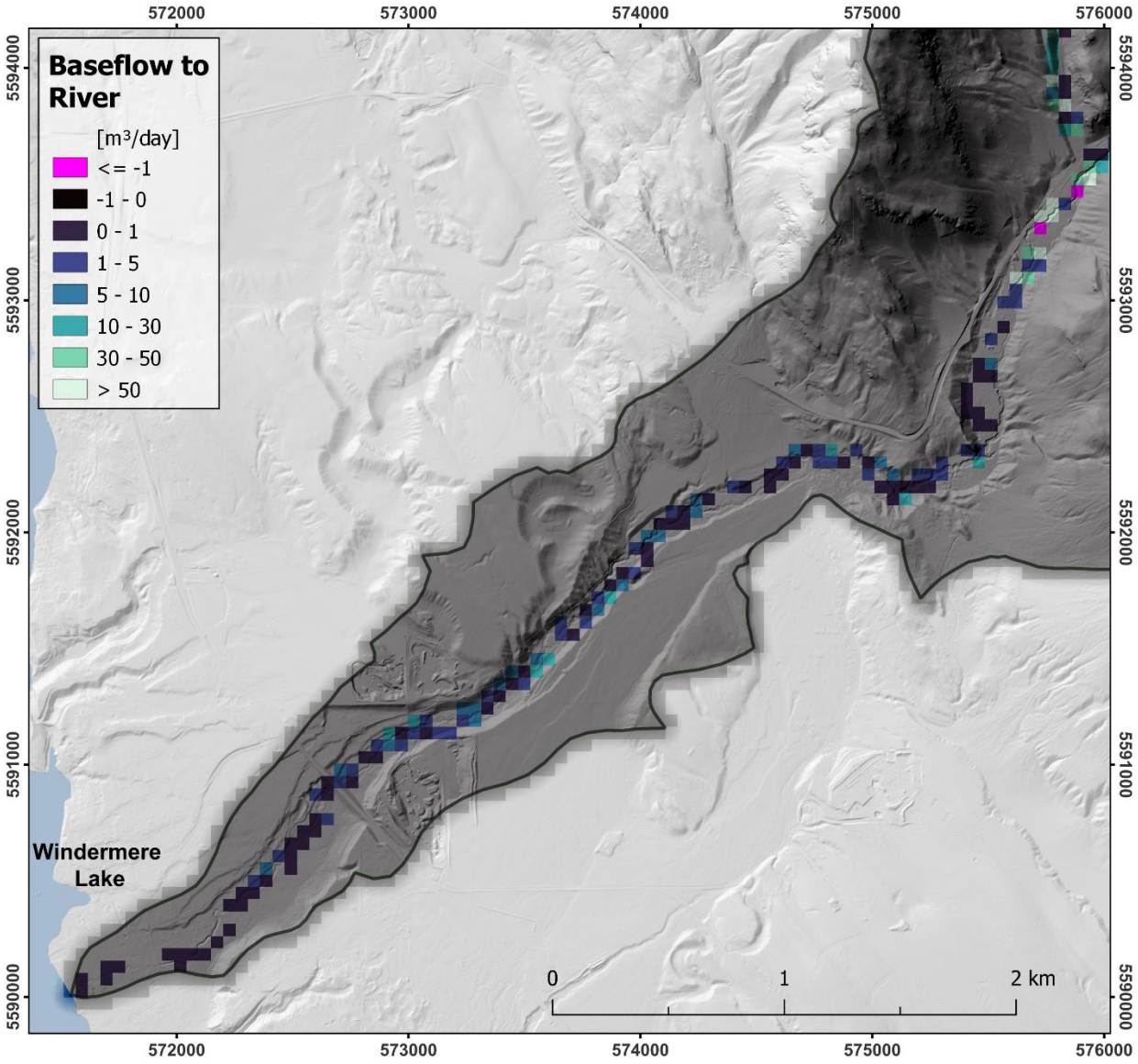

Figure 33. Average October baseflow contributions from groundwater to Windermere Creek in the fan area.

3.7 Wet vs. Dry Water Year

The model results for two water years (WY) were explored to represent wet versus dry conditions: the wet year 2018-2019 (referred to as the 2019 WY) and the dry year 2021-2022 (2022 WY). The 2019 WY received around 831 mm of precipitation versus about 391 mm in the 2022 WY. This difference was most apparent in the July to September period (Figure 34). In the 2022 WY, precipitation was almost half of what fell during the 2019 WY. This had significant effects on the amount of water transferred to the SZ (recharge). Interestingly, transfers from the SZ to the river remained quite high at 272 mm in 2022 compared to about 334 mm in 2019. Subsurface storage changes in the UZ and SZ, however, were quite different. During the 2019 wet WY, there was an increase of 136 mm in subsurface storage. However, the 2022 dry water year had a decrease of 148 mm. Thus, a large quantity of subsurface storage was released to maintain evapotranspiration and baseflow rates.

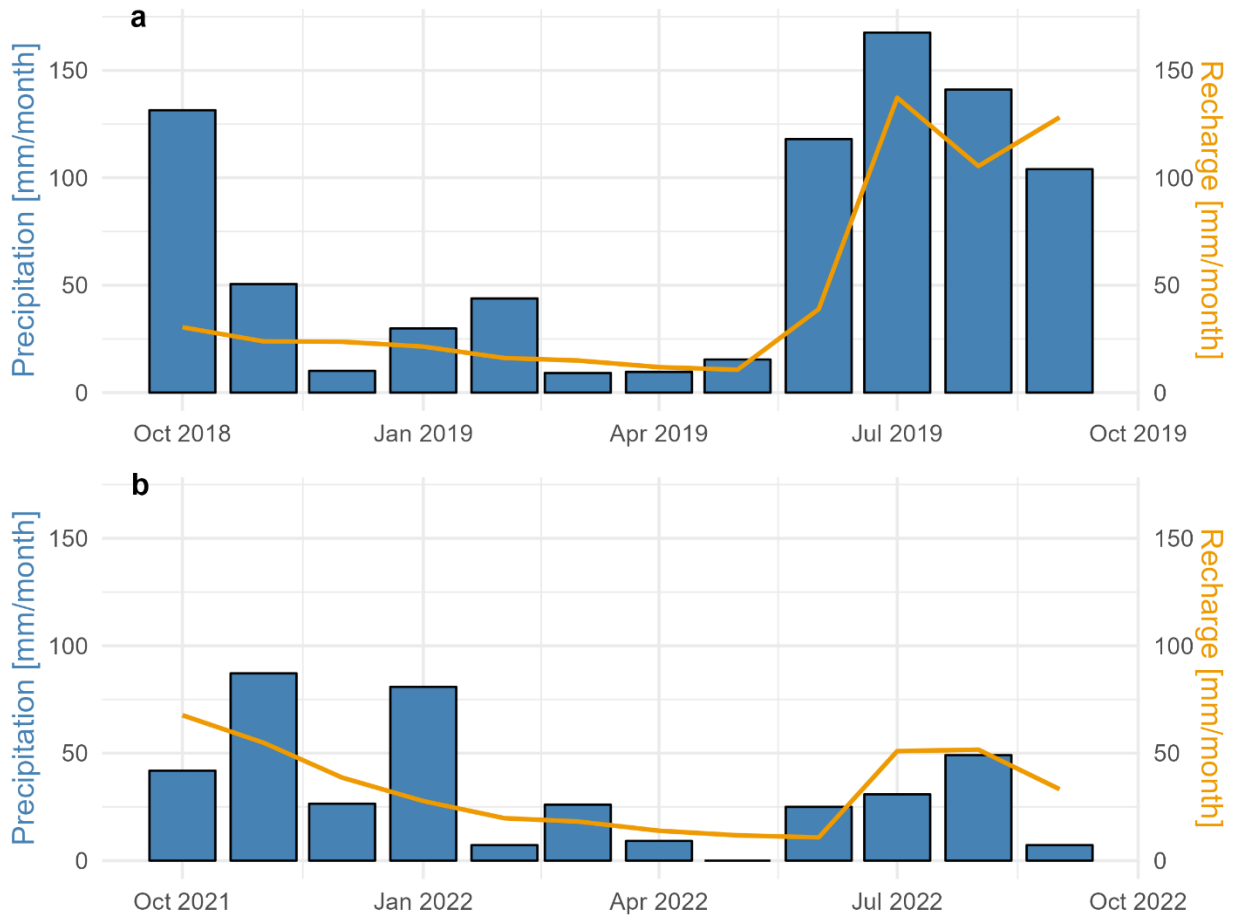

Figure 34: Precipitation (blue bars) and transfers to the SZ (recharge: yellow line) for (a) the 2019 wet WY and (b) the 2022 dry water year.

There was no obvious change in the depth to the water table in the 2019 wet WY (Figure 35) versus the 2022 dry WY (Figure 36). The water table was shallower in 2019, especially at the mountain front, where there were more blue cells (water table at or above ground surface). There may have been a reduction in groundwater spring flow in 2022, but this would need to be confirmed by local residents. In the mountain block, the water table was much lower in the ridges (not shown) in 2022.

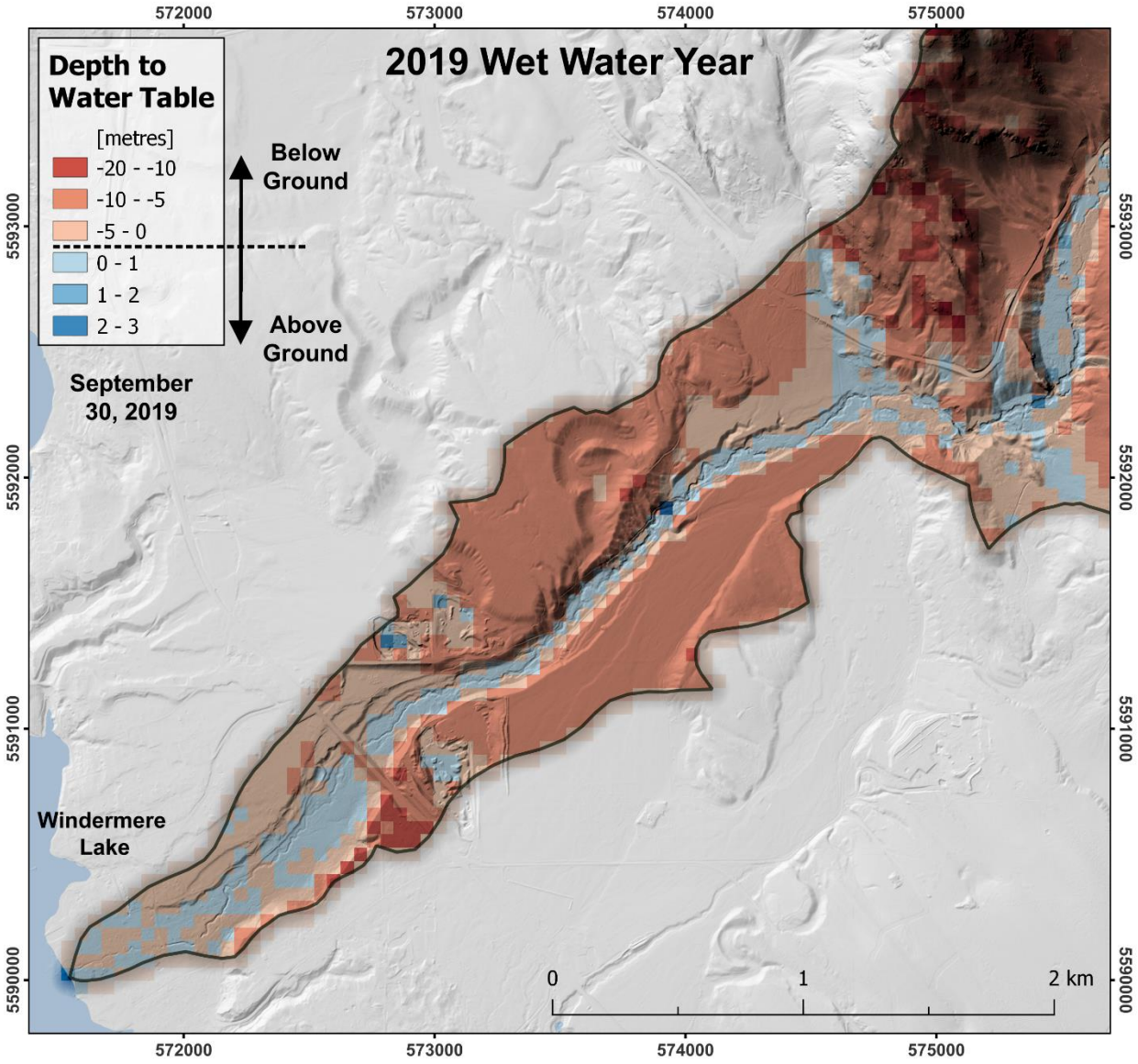

Figure 35: Depth to the water table in the fan area at the end of the 2019 wet water year (Sept 30).

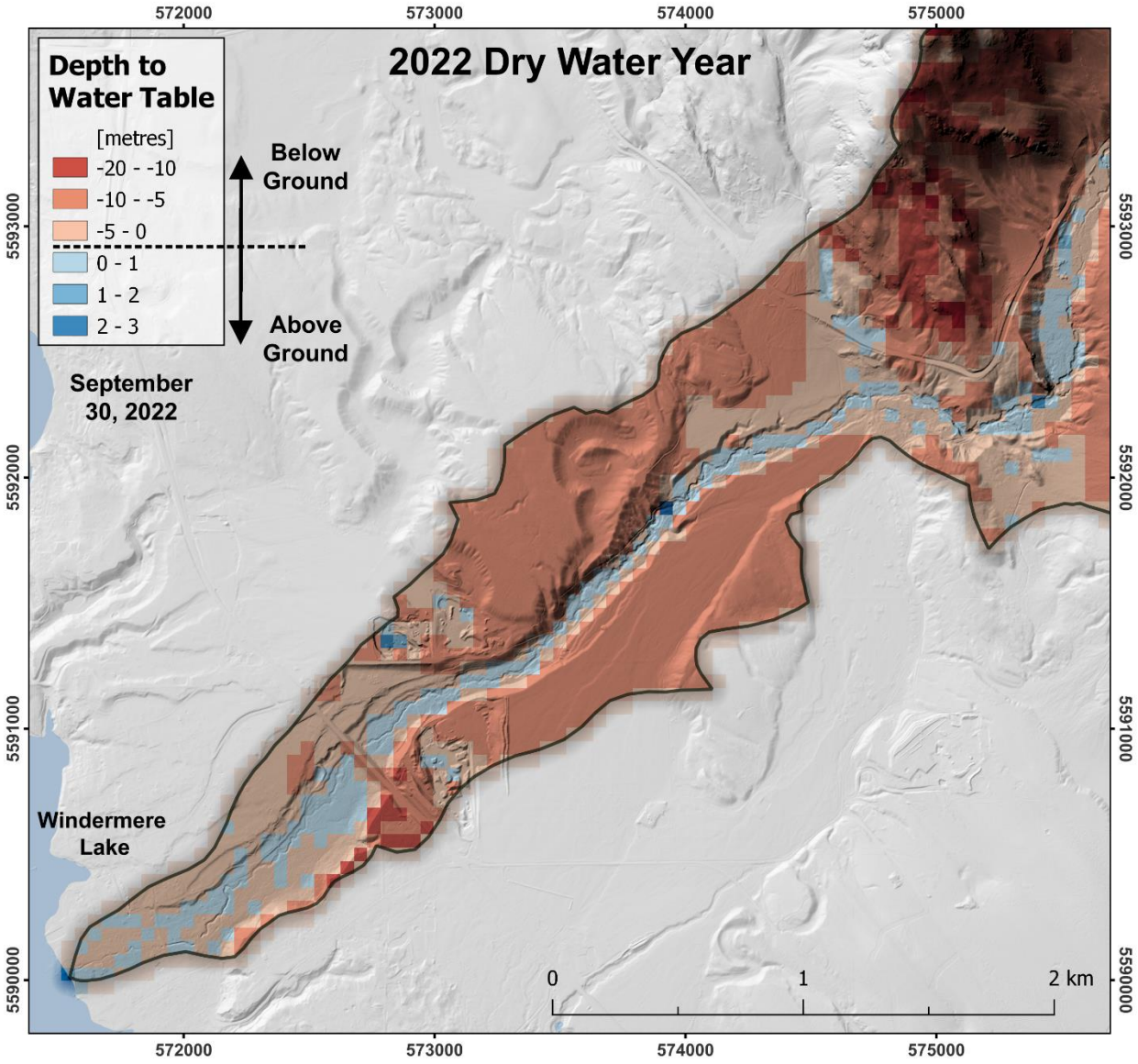

Figure 36: Depth to the water table in the fan area at the end of the 2022 dry water year (September 30).

4. DISCUSSION

4.1 Groundwater Recharge and Discharge

The complex and variable topography of the WCW proved to be particularly challenging to model, despite the relatively coarse grid cell size. The stream is just over 16 km long, with its headwaters at approximately 1,600 masl and the outlet at Windermere Lake at approximately 800 masl. The stream gradient is relatively constant through much of its length, even with a large change in elevation (Figure 37). The stream is deeply incised in the valley that cuts across the fan, terminating at the lake. This deep incision is a likely factor in effective stream-aquifer connectivity. In fact, the water table is consistently at or slightly above ground surface in most of the valley, meaning the stream is likely well connected to the fan aquifers.

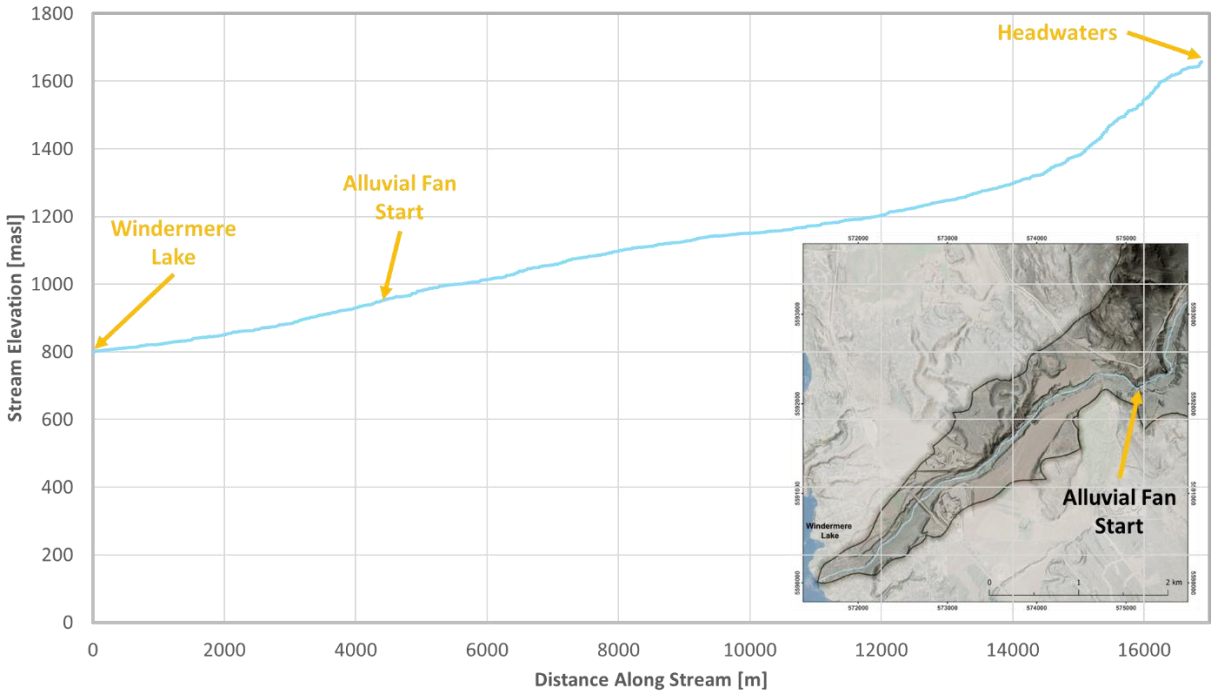

Figure 37: Windermere Creek gradient from the headwaters to the outlet at Windermere Lake.

Within the mountain block portion of the catchment, bedrock topography within the stream valleys plays a large role in shaping the stream path. Notably, there is a large and forced meander of the stream as it enters the fan apex (Figure 38). This is the result of the underlying bedrock topography that acts as a funnel for stream and groundwater flow. Groundwater flow velocities tend to be higher (Figure 20) at this groundwater bottleneck, and the water table was high enough to favour wetland conditions (Figure 38).

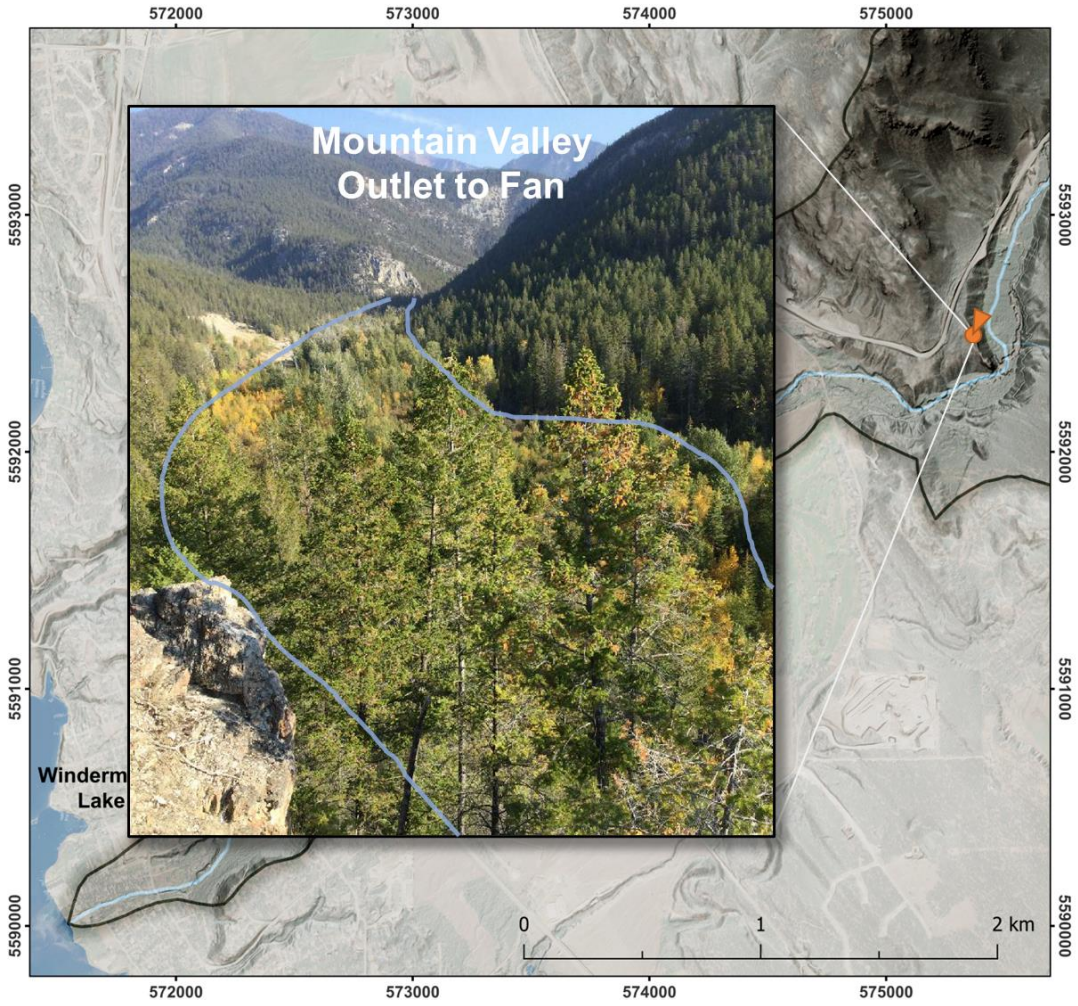

Figure 38: Wetland located where the stream transitions from the mountain valley to the fan. Photo courtesy of Natasha Neumann (October 2022).

4.2 Groundwater Use and Climate Change

There are two mapped aquifers that transect the WCW, each with a single licensed groundwater user:

1. Aquifer 1000, which is a confined fractured sedimentary rock aquifer (*Figure 10*: Unit CmOM). There is a single reported licensed well (WTN 117761) located within the WCW; and

2. Aquifer 453, which is a confined sand and gravel (Figure 14: Lower aquifer model layer). There is a single reported licensed well (WTN 118037) located outside of the WCW.

There are also 16 domestic wells within the bounds of the watershed, mostly at the catchment outlet by the lake.

At the scale of this model, the effects of pumping from so few wells would likely be minimal or imperceptible. Nevertheless, it is important to acknowledge that groundwater abstraction was not included in this simulation.

A concern was raised by local residents in 2018 that some domestic wells in the Windermere Loop Road area had gone dry. While this cluster of wells is outside of the WCW, some insights can be derived from the topography and underlying geology (Figure 39). Sediment thickness at the fan apex is quite thin but thickens to more than 60 m south of the watershed boundary (refer to inset cross-section). However, based on the bedrock configuration and simulated groundwater flow direction, the cluster of wells is likely not receiving any groundwater contribution from the WCW. In fact, because groundwater flow is bottlenecked at the mountain front and is being funneled by bedrock towards the fan apex, groundwater flow is likely perpendicular to this cluster of wells. This cluster of wells outside of the WCW is ultimately being influenced by a separate catchment, which is much smaller in area, with limited alpine extent (see Figure 1). Additionally, depth to bedrock is much larger with more accommodation space for sediment fill. Based on reported static water levels, the water table is much deeper here, around 30 m deep (GW Solutions, 2021).

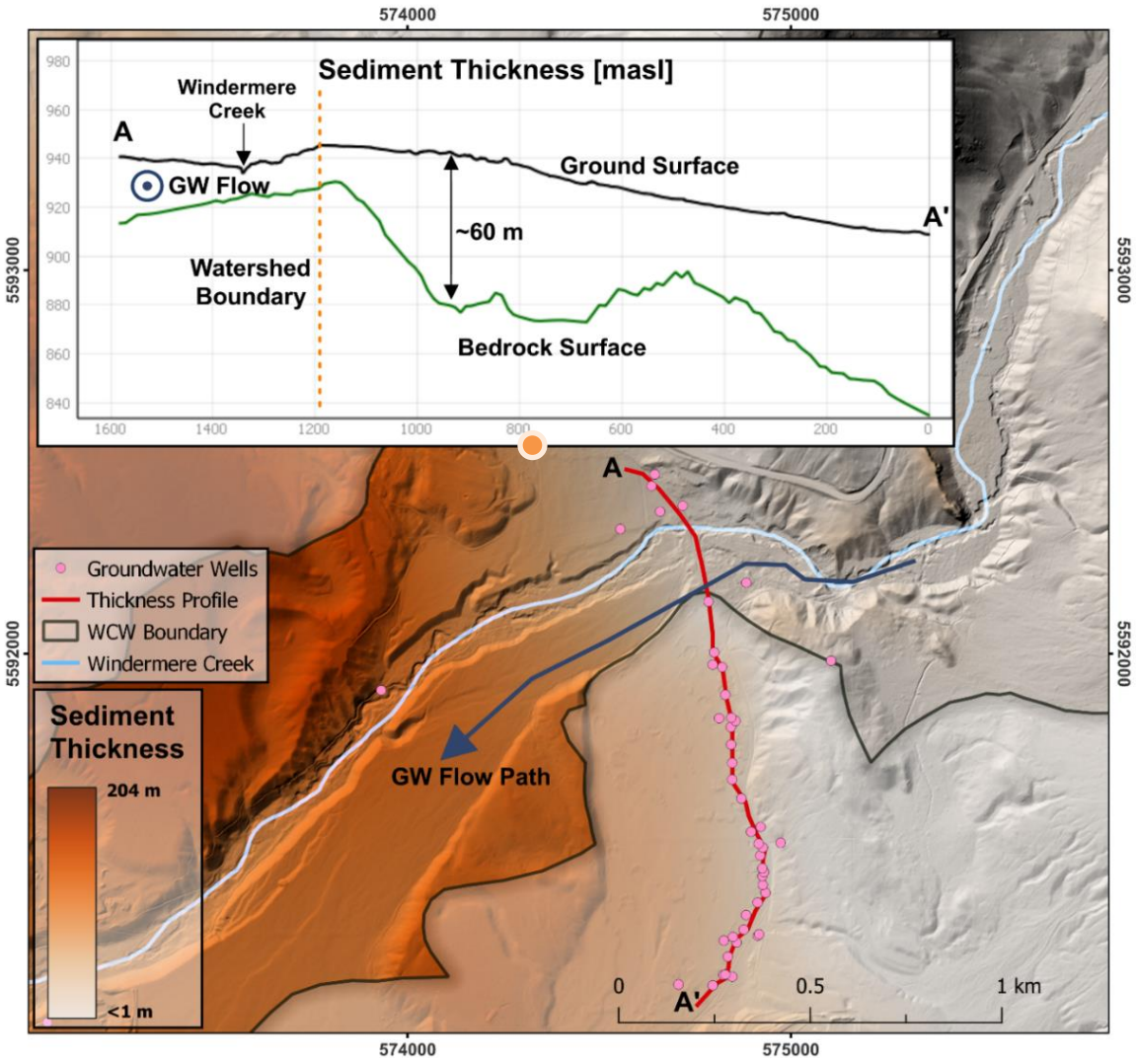

Figure 39. Sediment thickness at the fan apex at the mountain front. Note that groundwater flow is out of the page in the inset plot. Pink points represent all groundwater wells currently in GWELLS. The orange dot represents a point for which a time series was extracted, shown in Figure 25a.

The depth to the water table is generally within 5 m of ground level at the fan apex (Figure 22), but it is apparent in the modelling results when domestic wells may have gone dry within the WCW; in 2018, at the end of 2021, and mid 2022 to present, based on groundwater levels extracted at the fan apex (Figure 25a). Recharge rates in recent years (2018 to present) have been lower than during the 2014 to 2017 period, despite consistent snow water equivalent (SWE) amounts over the entire simulation period (Figure 17a). However, it must be noted that the observed and simulated SWE results are for SWE at high elevation (around 2000 masl). Transfers to the SZ (recharge) over the entire catchment declined in recent years (Table 6). Concurrently, changes in subsurface storage magnitudes increased (Table 6). Exchanges from the SZ to the stream also declined, likely caused by reductions in transfers to the SZ (recharge).

Recent groundwater level decline at the fan apex (Figure 25a) may be driven by a decline in recharge (Table 6) that is influenced by a reduction in the snowpack at both high and low elevations. Snowpack amount is intimately influenced by precipitation amounts and temperature. For example, the very dry 2022 water year received just over 50% of typical precipitation amount. About 45% of precipitation in the 2022 water year was converted to evapotranspiration, as opposed to the modelled average of 31%. As a result, water year transfers to the SZ (recharge) were at their lowest.

Snowpacks are important for delaying the timing and magnitude of water inputs to both streams and aquifers. Rasouli et al. (2022) show that increases in precipitation at higher elevations can offset the impact of warming on snowpack melt. However, at lower elevations more rain is expected near the phase transition temperature (i.e., the melting point of ice). Lower elevations of headwater basins in the Canadian Rockies are projected to shift towards a rainfall regime as precipitation shifts from falling as snow to falling as rain at low and mid-elevations (Rasouli et al., 2019). At these elevations peak SWE will decrease, with later snowpack initiation and a greater number of snow-free days. Hale et al. (2023) report that in the Canadian Rockies, earlier snowmelt has caused an earlier shift in water inputs to streams. Figure 40 shows the day of the year when the maximum SWE was attained at the Floe Lake station. While the trend is not statistically significant, it does seem that in recent years, snowmelt has begun a few days earlier.

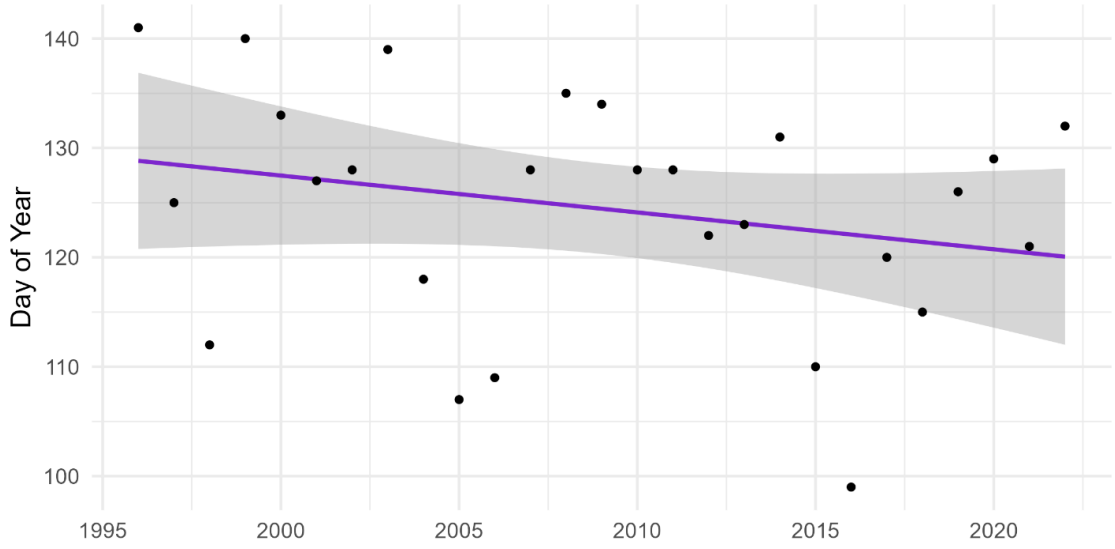

Figure 40. Day of the year when max SWE was attained at the Floe Lake station. A linear trend of -0.11 days/year in max SWE timing is not statistically significant (p = 0.791). As reference, April 30th is the 120th day of the year.

CONCLUSIONS AND RECOMMENDATIONS

A three-dimensional integrated hydrological model of WCW was constructed in MIKE SHE to elucidate spatiotemporal patterns of surface and groundwater interactions at a watershed scale. Unfortunately, there is no direct interface or intuitive method of bringing a LeapFrog model into MIKE SHE as both softwares are proprietary. Therefore, we had to develop a novel approach for representing the subsurface in MIKE SHE, which required substantial workarounds to import the geology into MIKE SHE via the use of geological lenses. The approach we developed, and which is described in this report, is transferrable to other modelling initiatives. Several challenges posed significant obstacles in successfully implementing and calibrating the final model:

1. **Subsurface Parameterization**: No studies or available data exist on the hydraulic and physical parameters (i.e., hydraulic conductivity and storage) paramount to accurately representing the soils, aquifers, and streambed sediments. Models are particularly sensitive to hydraulic conductivity.

2. **Lack of Calibration Data**: No modern timeseries data for groundwater, snow, climate, or streamflow was available within the bounds of the catchment. Climate and snow data were derived from nearby sources. Streamflow was monitored decades ago and thus gives only limited insight into modern processes. Groundwater in one well is synoptically monitored nearby, which did provide some insight into possible patterns, but was ultimately of no use in the model.

3. **Mountain Front Processes**: An attempt at expanding the original model domain was made to better capture mountain front processes related to the triangular facets of the mountain faces as well as incorporating more domestic well users. Ultimately, the model was unstable and failed to properly run as overland flow was not properly being routed, defeating the purpose of a well-defined topographic catchment boundary.

Despite the lack of a conventional calibration process, the final model appeared to capture the seasonality and large-scale spatial patterns of groundwater levels and flow patterns. While the recharge amount (transfers to the SZ) generated by the UZ water balance in MIKE SHE was undoubtedly over-estimated, a more realistic estimate of recharge was calculated using the individually modelled components of the model (AET and I). This water balance calculation suggests that recharge was on the order of 60% of precipitation. Unfortunately, baseflow to the river was consistently underestimated, although peak flows and flow recessions followed the expected patterns of timing. Actual evapotranspiration (AET) accounted for about 31% of precipitation while overland (OL) flow accounted for about 20%.

The modelling results suggested that Windermere Creek was consistently gaining water from groundwater in both space and time. In the fan area, there was likely strong hydraulic connectivity between the fan aquifer and Windermere Creek; however, the spatial and temporal exchanges could not be resolved with a model of this scale (50 m grid size). There are likely localized exchanges within the stream that could be resolved if a smaller scale model was developed for the fan area. The model also seemed to be able to show groundwater seepage zones especially in the stream valley within the fan and the wetland area at the fan apex.

Overall, the WCW is severely data starved. A local scale model of the fan, more appropriate for exploring fish habitat suitability and localized interactions between aquifers and the stream, would require

substantial physical and timeseries data. Without a large data collection campaign, attempting to model local scale processes is futile. Here, we suggest several recommendations to meet this goal:

1. **Monitor the Snowpack:** The model showed that snowpack processes are very important for modelling stream and groundwater processes. Ideally, one station on the fan and one at a higher elevation of the mountain block should be established and monitored.

2. **Establish Permanent Groundwater Monitoring Wells:** Groundwater should be regularly monitored, especially near the stream, to capture the seasonality and response to precipitation in both shallow and deep aquifers.

3. **Install Streambed Piezometers and Streamflow Gauges:** Gauges should be established at different locations along the stream to identify gaining versus losing reaches. Streambed piezometers could also be used for determining vertical directions in aquifer-stream exchanges.

REFERENCES

Allen, D.M. and Nott, A.H. (2021) How important are those fracture zones? Scale dependent characteristics revealed through field studies and an integrated hydrological model of a mountain headwater catchment. Frontiers in Water, 3. Special Issue Uncertainty in Groundwater Modeling Across Scales.

Allen, R. G., Pereira, L. S., Raes, D., and Smith, M. (1998). Crop evapotranspiration: Guidelines for computing crop water requirements, FAO irrigation and drainage paper 56, Rome: FAO, 328 pp.

B.C. SIFT (2018) BC SIFT Soil Polygons, Provincial Soils Working Group, BC Ministry of Environment and Climate Change Strategy and Ministry of Agriculture.

B.C. Geological Survey (BCGS) (2019) BC Digital Geology - BC Geological Survey - Province of British Columbia. https://www2.gov.bc.ca/gov/content/industry/mineral-exploration-mining/british-columbia-geological-survey/geology/bcdigitalgeology. Accessed 21 Mar 2023

Carsel, R.F., and Parrish, R.S. (1988) Developing joint probability distributions of soil water retention characteristics. Water Resources Research, 24, 755–769. https://doi.org/10.1029/WR024i005p00755

Chen, J.M., Pavlic, G., Brown, L.., Cihlar, J., Leblanc, S.G., White, H.P., Hall, R.J., et al. (2002) Derivation and validation of Canada-wide coarse-resolution leaf area index maps using high-resolution satellite imagery and ground measurements. Remote Sensing of the Environment, 80, 165–184. https://doi.org/10.1016/S0034-4257(01)00300-5

Danish Hydraulic Institute (2022). MIKE SHE software, Danish Hydraulic Institute: Denmark.

Foster, S.B., Allen, D.M., 2015. Groundwater—Surface Water Interactions in a Mountain-to-Coast Watershed: Effects of Climate Change and Human Stressors. Advances in Meteorology 2015, e861805. https://doi.org/10.1155/2015/861805

ESRI HYDRO (2020) Average Annual Evapotranspiration. https://www.arcgis.com/sharing/rest/content/items/ad3f8cc18fc74e6894ee220acd15020a (Accessed 7 Jun 2023).

GeoBC (2021) Open LiDAR Data Portal. In: LidarBC - Open LiDAR Data Portal. https://governmentofbc.maps.arcgis.com/apps/MapSeries/index.html?appid=d06b37979b0c4709b7fcf2a1ed458e03. (Accessed 7 Jul 2022).

GeoBC (2020) Digital Elevation Model for British Columbia - CDED - 1:250,000 - Datasets - Data Catalogue. https://catalogue.data.gov.bc.ca/dataset/digital-elevation-model-for-british-columbia-cded-1-250-000. (Accessed 6 Apr 2023).

GeoBC (2023) Freshwater Atlas Stream Network – BC Data Catalogue. In: BC Freshwater Atlas Stream Network. https://catalogue.data.gov.bc.ca/dataset/freshwater-atlas-stream-network. (Accessed 11 Apr 2023).

GW Solutions Inc. (2021) Windermere Preliminary Hydrogeological Characterization. Living Lakes Canada and The Gordon Foundation.

GWELLS (2023) Groundwater Wells and Aquifers - Province of British Columbia. https://apps.nrs.gov.bc.ca/gwells/. (Accessed 21 Mar 2023).

Hale KE, Jennings KS, Musselman KN, et al (2023) Recent decreases in snow water storage in western North America. Commun Earth Environ 4:1–11. https://doi.org/10.1038/s43247-023-00751-3

Harter, T. (2005) Specific yield storage equation. In: Water Encyclopedia. John Wiley & Sons, Ltd, pp 576–578.

Kristensen, K., and Jensen, S. (1975). A model for estimating actual evapotranspiration from potential evapotranspiration. Nordic Hydrology, 6(3), 170-188.

Kuang, X., Jiao, J.J., Zheng, C., Cherry, J.A., and Li, H. (2020) A review of specific storage in aquifers. Journal of Hydrology, 581, 124383. https://doi.org/10.1016/j.jhydrol.2019.124383

Linsley, R.K., Kohler, M.A., Paulhus, J.L.H. (1982) Hydrology for Engineers. McGraw-Hill.

Living Lakes Canada (LLC) (2023) Living Lakes Groundwater Monitoring Program - Columbia Basin Water Hub. https://data.cbwaterhub.ca/organization/living-lakes-groundwater-monitoring-program (Accessed 21 Mar 2023).

Lindsay, J.B., Dhun, K., 2015. Modelling surface drainage patterns in altered landscapes using LiDAR. International Journal of Geographical Information Science 29, 397–411. https://doi.org/10.1080/13658816.2014.975715

Lindsay, J.B., 2016. Whitebox GAT: A case study in geomorphometric analysis. Computers & Geosciences 95, 75–84. https://doi.org/10.1016/j.cageo.2016.07.003

NASA POWER (2023) The POWER Project. https://power.larc.nasa.gov/ (Accessed 17 Mar 2023)

Natural Resources Canada (NRCAN) (2019) 2015 Land Cover of Canada. https://open.canada.ca/data/en/dataset/4e615eae-b90c-420b-adee-2ca35896caf6 (Accessed 17 Mar 2023)

Paudel, S. (2021) Impact of Precipitation Sources on Surface Water and Groundwater Hydrology in the Canteen-Cahokia Watershed, IL, USA. M.Sc. thesis, Southern Illinois University at Edwardsville. https://www.proquest.com/docview/2542366413?pq-origsite=gscholar&fromopenview=true (Accessed 31 March 2023).

Rasouli K, Pomeroy JW, Whitfield PH (2019) Hydrological Responses of Headwater Basins to Monthly Perturbed Climate in the North American Cordillera. Journal of Hydrometeorology 20:863–882. https://doi.org/10.1175/JHM-D-18-0166.1

Rasouli K, Pomeroy JW, Whitfield PH (2022) The sensitivity of snow hydrology to changes in air temperature and precipitation in three North American headwater basins. Journal of Hydrology 606:127460. https://doi.org/10.1016/j.jhydrol.2022.127460

Seequent (2022) Leapfrog Geo 2022.1. https://help.seequent.com/Geo/2022.1/en-GB/Content/intro.htm. Accessed 12 Apr 2023

Shao, Y., and Irannejad, P. (1999) On the choice of soil hydraulic models in land-surface schemes. Boundary-Layer Meteorology, 90, 83–115. https://doi.org/10.1023/A:1001786023282

Sharma, P.V. (1997) Environmental and Engineering Geophysics. Cambridge University Press, Cambridge

Thompson, J. R., Sørenson, H. R., Gavin, H., and Refsgaard, A. (2004). Application of the coupled MIKE SHE/MIKE 11 modelling system to a lowland wet grassland in Southeast England. Journal of Hydrology, 293(1–4), 151-179. doi: http://dx.doi.org/10.1016/j.jhydrol.2004.01.017

Vionnet, V., Mortimer, C., Brady, M., Arnal, L., and Brown, R. (2021) Canadian historical Snow Water Equivalent dataset (CanSWE, 1928–2020). Earth Syst Sci Data 13:4603–4619. https://doi.org/10.5194/essd-13-4603-2021

Voeckler, H.M., Allen, D.M., Alila, Y. (2014) Modeling coupled surface water – groundwater processes in a small mountainous headwater catchment. Journal of Hydrology, 517, 1089–1106. https://doi.org/10.1016/j.jhydrol.2014.06.015

Welch, L.A. and Allen, D.M. (2014) Hydraulic conductivity characteristics in mountains and implications for conceptualizing bedrock groundwater flow. Hydrogeology Journal 22(5): 1003-1026.

Yang, Y., Donohue, R.J., and McVicar, T.R.(2016) Global estimation of effective plant rooting depth: Implications for hydrological modeling. Water Resources Research, 52, 8260–8276. https://doi.org/10.1002/2016WR019392

Zotarelli, L., Dukes, M., Romero, C., Migliaccio, K., and Kelly, T. (2015) Step by Step Calculation of the Penman-Monteith Evapotranspiration (FAO-56 Method) 1. https://www.semanticscholar.org/paper/Step-by-Step-Calculation-of-the-Penman-Monteith-1-Zotarelli-Dukes/8c7a164802368a05710ade7acc0f38d9b136f8be (Accessed 31 March 2023).